INVESTIGATION OF CERAMICS FOR HIGH-TEMPERATURE TURBINE VANES

Svante Prochazka

General Electric Corporate Research and Development

Prepared for:

Naval Air System Command

31 December 1972

INVESTIGATION OF CERAMICS FOR HIGH-TEMPERATURE TURBINE VANES

FINAL REPORT

December 1972

by

Svante Prochazka

Prepared Under Contract N00019-72-C-0129

for

Department of the Navy
Naval Air System Command
Washington, D. C. 20360

General Electric Company
Corporate Research & Development
P.O. Box 8, Schenectady, New York 12301

SRD-72-171

UNCLASSIFIED

Security Classification

DOCUMENT CONTROL DATA - R & D

(Security classification of title, body of abstract and indexing annotation must be entered when the overall report is classified)

1. ORIGINATING ACTIVITY (Corporate author)
General Electric Company
Corporate Research and Development
Schenectady, New York 12301

2a. REPORT SECURITY CLASSIFICATION
UNCLASSIFIED

2b. GROUP

3. REPORT TITLE
INVESTIGATION OF CERAMICS FOR HIGH TEMPERATURE TURBINE VANES

4. DESCRIPTIVE NOTES (Type of report and inclusive dates)
Final Report - April 1, 1972 - December 13, 1972

5. AUTHOR(S) (First name, middle initial, last name)
Svante Prochazka

6. REPORT DATE
December 31, 1972

7a. TOTAL NO. OF PAGES
32 68

7b. NO OF REFS
29

8a. CONTRACT OR GRANT NO
N00019-72-C-0129

b. PROJECT NO

c.

d.

9a. ORIGINATOR'S REPORT NUMBER(S)
SRD-72-171

9b. OTHER REPORT NO(S) (Any other numbers that may be assigned this report)

10. DISTRIBUTION STATEMENT
Approved for Public Release. Distribution Unlimited.

11. SUPPLEMENTARY NOTES
Details of illustrations in this document may be better studied on microfiche

12. SPONSORING MILITARY ACTIVITY
Naval Air System Command
Washington, D. C. 20360

13. ABSTRACT

The objective of this work has been to investigate those parameters which limit the mechanical properties of SiC at high temperatures. The main approach utilized in this work has been to optimize processes and compositions for the base structural ceramic, SiC, such that appropriate microstructures could be obtained by hot-pressing at low pressures. These materials are then subjected to high-temperature mechanical tests.

The results show that carbon reduction of amorphous silica containing 0.5% boron at 1650° to 1800° temperatures in argon will yield submicron β-SiC powders well sinterable under nominal hot pressing conditions. Three different microstructures are obtained, depending on whether the powders are oxidized in air at 700°C, oxidized and leached with HF, or blended with hyperstoichiometric carbon additions. Of the three, the latter obtained with excess carbon additions is shown to be the preferred structure.

In addition, measurements of three point bending strength up to 1600°C, creep rate, delayed failure, and oxidation rate at 1600°C show improvements are obtained by these small carbon additions. At this temperature, strengths in excess of 60 Kpsi have been developed.

DD FORM NOV. 1473

UNCLASSIFIED

Security Classification

14 KEY WORDS	LINK A		LINK B		LINK C	
	ROLE	WT	ROLE	WT	ROLE	WT
Silicon Carbide						
Hot-Pressing						
Strength						
Creep						
Delayed Fracture						
Oxidation Resistance						
Crack Size						
Microstructure						
Grain Growth						

TABLE OF CONTENTS

FOREWORD

The research work reported herein was conducted by the Metallurgy and Ceramics Laboratory of GE Corporate Research and Development under NASC Contract N00019-72-C-0129. Mr. Irving Machlin of the Naval Air System Command was the responsible monitor. Dr. Svante Prochazka was the principal investigator of the program and the work was performed within the Ceramics Branch, Dr. R.J. Charles, Manager.

The author would like to express his appreciation to W.J. Dondalski and Carl Bobik for technical assistance, to Ed Koch for exceptional metallographic work, and to many of the Laboratory staff for helpful discussions. We would like also to thank Dr. H.S. Spacil for thermodynamic calculations and to P.C. Smith for the view of the manuscript.

ABSTRACT

The objective of this work has been to investigate those parameters which limit the mechnical properties of SiC at high temperatures. The main approach utilized in this work has been to optimize processes and compositions for the base structural ceramic, SiC, such that appropriate microstructures could be obtained by hot-pressing at low pressures. These materials are then subjected to high-temperature mechanical tests.

The results show that carbon reduction of amorphous silica containing 0.5% boron at 1650° to 1800° temperatures in argon will yield submicron β-SiC powders well sinterable under nominal hot pressing conditions. Three different microstructures are obtained, depending on whether the powders are oxidized in air at 700°C, oxidized and leached with HF, or blended with hyperstoichiometric carbon additions. Of the three, the latter obtained with excess carbon additions is shown to be the preferred structure.

In addition, measurements of three point bending strength up to 1600°C, creep rate, delayed failure, and oxidation rate at 1600°C show improvements are obtained by these small carbon additions. At this temperature, strengths in excess of 60 Kpsi have been developed.

1. INTRODUCTION

Gas turbine inlet temperatures have been increased well beyond the stability limits of superalloys by the development of intricate cooling systems. Limitations have been reached, however, and any further steps will require higher permissible component temperatures. With the potential of metals nearly exhausted, ceramics become interesting inspite of their shortcomings with respect to brittle behavior. Vanes have been selected as the first ceramic turbine components to be developed and tested since they are exposed to the highest temperatures, are more difficult to cool than other parts and do not require the extreme mechanical properties typical for blade materials. Silicon nitride vanes are scheduled for full scale testing in a 30 MW land based power generation unit under the auspices of an ARPA program. Extensive evaluation of high grade hot-pressed Si_3N_4 initiated in this program confirmed its outstanding properties at room and moderate temperatures but also its limitations above 1400°C (2500°F) in strength and oxidation resistance. It is now generally accepted that for temperatures above 1400°C silicon carbide is the best and probably the only current candidate material.

The goal of this program has been the development of a ceramic with the highest possible strength for turbine applications up to 3000°F. The high strength requirement arrises from the need of the material to sustain thermal stresses generated on turbine shut down and from requirements of impact resistance. A meaningful level of impact properties, however, would require a tensile strength near 300,000 psi. To generate such a strong ceramic in bulk is a formidable problem compounded by the presently limited understanding of fracture initiation processes in this material. Nevertheless, it is probably not an impossible task since even higher strengths have been observed in polycrystalline CVD fibers made of SiC.

It is believed that SiC has the highest potential of any known compound and that a dense, single phase, fine grained, high purity form will yield the desired ceramic. Its strength will be controlled by various factors that determine the local stress level at fracture such as microscopic inhomogenieties, surface flaws, grain size or microplastic yielding. Our work is an effort to understand and control these factors.

A powder composition and a hot pressing process for consolidation of SiC into an essentially single phase pore free ceramic was devised in the first year of the program.[1]

1. It was shown that small amounts of boron aid in the densification of SiC at nominal hot-pressing conditions and fine grained microstructures were generated. Bending strengths in excess of 100,000 psi at room temperature and 64,000 psi at 1500°C were demonstrated and oxidation resistance was found to be excellent up to 1600°C. This ceramic was made by pressure sintering of a submicron size fraction of an SiC powder separated by sedimentation from

a high grade commercial SiC (E277). Densities above 99% of the theoretical with a uniform 3.2 micron grain size microstructure could be routinely obtained at 1950°C, 10,000 psi in 30 minutes. At 2000°C and above, exaggerated grain growth was observed and attributed to a silicon melt formation.

At this stage further plans toward process optimization, scaling up and characterization of the material at high temperatures were modified in order to avoid possible variabilities of commercially available SiC materials. Investigation into the techniques of SiC powder preparation was therefore included in this year's program in order to assure the use of pure, submicron SiC powders. This approach also had the potential of eliminating the inconvenience of fine grinding, leaching, fractionation and small yields, typical in the preparation of submicron powders by comminution.

It has been shown in nearly all of the recent developments in ceramic hot pressing that powder properties such as grain size, size distribution, grain shape, crystalline structure and trace chemical composition play an extremely important role in determining the microstructure and resulting mechanical behavior. Thus while the decision to produce in-house powders temporarily brought about the difficulty of using unstabilized powders for hot-pressing experiments it subsequently yielded an important fundamental understanding of the requirements for a sinterable SiC powder. The main objective was to obtain an improvement and understanding of high temperature strength of SiC and this is sensitively dependent on raw materials characteristics. For example, recent investigations of the mechanical properties of hot-pressed SiC made elsewhere[2, 3] indicate a drastic degradation of strength above 1400°C contrary to the behavior of CVD SiC and single crystals.[4, 5] It was, therefore, essential to resolve this difference and to establish the processing potential of material densification by hot-pressing procedures. Progress towards this objective and all the other tasks are summarized below. The work is covered in three sections dealing with the three major aspects of the investigations: powder preparation, hot-pressing and microstructure control and mechanical properties measurement.

2. SUMMARY OF SIGNIFICANT RESULTS

1. Submicron particle size SiC powder, suitable for hot-pressing operations, is prepared by firing an intimate hyperstoichiometric mixture of carbon and amorphous silica at 1650° to 1800°C in an atmosphere of 100 mm argon. Excess carbon is burnt off in air and silica is dissolved in HF. Boron is added (0.5%) as H_3BO_3 on preparation of the amorphous silica gel.

2. The powders could be hot-pressed to near theoretical densities at 1950°C and 10 Kpsi. They exhibited exaggerated grain growth in varying degrees which was later suppressed by a 1% carbon addition.

3. Exaggerated grain growth of large tabular crystals was linked to the β-α SiC transformation and would proceed by two different mechanisms. For both cases small amounts of oxygen and a silicon metal phase were involved. Carbon addition suppressed this anomalous grain growth probably by the removal of residual oxygen.

4. Three types of microstructures develop on hot-pressing of SiC depending on whether silica, silicon or carbon is present during densification. These microstructures exhibit a) uniform fine equiaxed grains, b) large tabular crystals in a fine grain matrix, and c) fine elongated SiC grains.

5. Strengths of 80,000 psi were determined by surface defects, introduced on diamond machining, at temperatures below 1400°C. At 1600°C slow crack propagation was observed as would be expected under these conditions. A 1% carbon addition increased strength at 1500°C by 25%.

6. Creep measurements yielded strain rates 1.2×10^{-8} and 1.5×10^{-9}/sec at 1600°C and 25,000 psi respectively. The increased strain rate was tentatively linked to small amounts of free silicon. On the other hand, a small amount of SiO_2 (1 vol/o) does not affect creep.

3. POWDER PREPARATION

3.1 Requirements and Methods of Preparation

Target powder properties were established mainly on the properties of the submicron powder prepared previously from the SiC E277 which yielded high densities and satisfactory microstructures on hot-pressing. These characteristics are listed in Table I. The oxygen content is high, 4.9%, and as will be shown below plays an important role in microstructure development. It is, however, not necessarily a harmful constituent. This powder is composed of isolated crystallites of a wide particle size distribution which are probably fragments obtained by grinding (no details on the fabrication of E277 were obtainable). For hot pressing this is a very desirable feature which usually cannot be obtained by a process based on thermal synthesis or chemical decomposition.

Three processes were selected for in-house submicron SiC preparation:

1. Comminution
2. Synthesis from the elements
3. Carbon reduction of SiO_2.

Several other processes were also considered such as formation of SiC in a plasma, thermal decomposition of organosilicon compounds and reactions of $SiCl_4$ with hydrocarbons. The latter processes, however, were though to be too prone to local and batch to batch variations to be practical.

TABLE I

CHARACTERISTICS OF TYPICAL SiC POWDERS

Powder Designation / Characteristic	SiC E277 -1μ	S-2 Synthesized From Si + C	M-1 Milling of Abrasive Grade SiC	D-6 SiO_2 Gel Reduction Unleached	ES-3 SiO_2 Gel Reduction Leached
Fe ppm	1500	800	2900	900	700
Al	1600	200	4000	150	100
B	60	500	80	4000	4600
Ca	20	50	280	—	40
O_2	4.9	—	—	4.9	0.59
Spec. Surface Area m^2/g	18.2	7.1	5.9	19.9	15.0
Mean Surface Average Particle Size, μ	0.1	0.29	0.33	0.1	0.13
X-ray Diffraction	β-SiC minor α-6H	β-SiC	α-SiC mixture of polytypes	β-SiC	β-SiC

3.2 Comminution of SiC

A sharp cut-off of the particle size distribution near 1 micron is essential for the preparation of uniform fine-grained microstructures in the low micron region. Hence ball-milling which typically produces a wide size distribution requires a subsequent particle size separation step. Wear of grinding media further complicates this approach and makes it a laborious and lengthy procedure. It has , however, the advantage of yielding a product free from clusters and strongly bonded aggregates.

Figure 1 shows the particle size distribution of a 600 mesh abrasive quality SiC after being wet ball milled with steel balls for 50 hours and subsequently acid leached and washed. The procedure takes several weeks but could be accelerated by electrodialysis. As shown, the yield of submicron particles was only about 10%. Another experiment with finer starting charge (1500 mesh SiC from Carborundum Co.) also yielded only 10% submicron SiC. Fluid jet milling was also tried but even smaller yields of fine particles were obtained. It was concluded that comminution of SiC to the desired submicron particle size in one step is not possible. However, if the requirement were to be relaxed to a -5μ, conventional ball milling might be a satisfactory procedure.

3.3 Synthesis of SiC from Its Elements

SiC forms readily from the elements on heating at about 1200°C but temperatures above the silicon melting point are necessary to bring the reaction in a Si + C powder mixture to completion. Under these conditions, carbon transport through silicon liquid is rate-controlling and in a fine dispersion, it is a rapid reaction.

A mixture of -325 mesh Si powder (Poly Research Corp., 99.99%) and acetylene black (Columbian Carbon Corp., 99.0% carbon) and 1% boron was reacted in argon atmospheres at 1500° and 1650°C. The reaction was followed by residual carbon analyses. The characteristics of the powder prepared at 1500°C are listed in Table I (Column 2) and the typical shapes of the powder particles are shown in Figure 2. There were always two distinct types of particles present:

a. Large porous clusters of rounded-off grains, 0.3 to 0.5 microns in size; and

b. Individual, mostly platelike crystals, up to several microns in size.

This bimodal morphology was typical. It was observed that particles with crystalline habit predominated at the surface of the reaction batch.

In the reaction, stoichiometric excess of carbon was used and the unreacted part was burned off in air at 700°C. The powders were subsequently leached by 25% HF to remove silica formed in the preceding step and finally ball milled with Carboloy balls to break up aggregates.

Hot-pressing experiments done with powders synthesized from Si and C showed poor "sinterability." For instance only 93.7% theoretical density was achieved at 2100°C and 10 Kpsi. The reason is not well understood; it may be connected to small amounts of unreacted silicon. It will be shown below, that the presence of elemental silicon affects densification. Work on synthesis from elements was discontinued.

3.4 SiC by Reduction of SiO_2

Preliminary experiments done according to a preparation method described by U.S. Patent 3085863 gave powders which were easily hot-pressed to high density. Therefore, this method was adopted and studied in more detail. The original procedure involves hydrolysis of silicon chloride in a sugar solution to form a gel which on drying and prefiring at 300°C yields amorphous silica intimately mixed with carbon. This precursor is then fired at 1800°C in argon to obtain β-SiC.

3.4.1 Preparation of the Gel

For present purposes the above procedure was modified in that silicon tetrachloride was replaced by ethylsilicate to eliminate the inconvenience of the vast amounts of HCl released on hydrolysis. $Si(OC_2H_5)_4$ reacts slowly at low P_H and at elevated temperatures so that the process is easily controlled.

By varying ethylsilicate to sugar ratios in the batches, the stoichiometry of the precursor (C/Si ratio) was adjusted between 3 to 4.5. The theoretical ratio was expected to yield pure SiC. However, in the absence of excess carbon, the reaction could never be completed and this was manifested by high (up to 11%) oxygen contents in the powders obtained on calcination. Moreover, a large loss of silicon was noticed and attributed to the reactions:

$$SiO_2 + C = SiO + CO \qquad (3.1)$$

$$SiC + 2\ SiO_2 = 3\ SiO + 2\ CO \qquad (3.2)$$

Microscopic examination of powders calcined at 1750°C revealed globules of fused silica in yellow SiC. It was concluded that on drying the gel, the contained sugar solution migrates to the surface of the gel particles and thus couses inhomogeneity in carbon distribution. The surface of the particles becomes carbon-rich and the depleted interior will eventually melt on calcination. The unreacted SiO_2, not being in contact with carbon, may then react according to the second equation.

Spray-drying of the diluted gel and grinding of the precursor was tried but did not improve the results. However, excess carbon was very beneficial and brought about high yields of SiC. A 25% excess of carbon gave satisfactory results in a series of 15 experiments. A typical batch consisted of:

500 cc ethylsilicate	2.5 g H_3BO_3
350 cc water	
500 g sugar	1 cc HCl

The components, when mixed, form initially two immiscible liquids which, on heating, gradually dissolve. After approximately one hour at 80°C, the solution turns into a transparent, colorless gel.

3.4.2 Calcination of the Precursor

The Si-C-O system is univariant in the presence of three solid phases, i.e., at a selected temperature the pressure of gas (SiO-CO-CO_2) and its composition is determined by phase equilibria. The thermodynamics of the system was investigated by Krivsky and Schuhman[6] and Poch and Dietzel.[7]

Figure 3 shows the gas pressure vs temperature relationship in the system. Curve II represents the coexistence of SiO_2-SiC-C-gas and Curve I that of SiO_2-SiC-Si-gas. The field between the curves gives the temperature and pressure conditions within which SiC may be formed from SiO_2 with the provision that the SiO/CO (and CO/CO_2) partial pressure ratio is sufficiently high. The reaction

$$SiC_{(s)} + 2\ SiO_{2(s)} = 3\ SiO_{(g)} + CO_{(g)} \qquad (3.3)$$

is nominally controlled by this SiO/CO ratio and a low value, in an open system, would lead to decomposition of SiC.

The pressure conditions for the reaction are most critical and may be discussed in terms of two pressure regimes, P_I and P_{II} (Figure 3). When the total gas pressure $P < P_I$ silicon and CO will form according to the reaction:

$$2\ SiC_{(s)} + SiO_{2(s)} = 3\ Si_{(l)} + 2CO_{(g)} \ . \qquad (3.4)$$

If $P > P_{II}$ silica will react with SiC according to the equation:

$$SiC_{(s)} + SiO_{2(s)} = C_{(s)} + 2\ SiO_{(g)} \ . \qquad (3.5)$$

The main problem of the control of SiC formation is that there are no practical means to monitor the SiO/CO partial pressure ratios in an open

system, i.e., to remove CO and hold back SiO. Therefore, the overall reaction:

$$SiO_{2(s)} + 3C_{(s)} = SiC + 2CO \qquad (3.6)$$

will never approach theoretical yield and some silicon will always be lost as SiO.

The gel was first dried to form a stiff mass which was broken into 1/8" pieces and heated to 300°C to complete drying and pyrolyze the sugar. The black precursor was calcined after that at 1650° to 1800°C in a carbon crucible. Higher temperatures were not applied because of coarsening of the product. The crucible was brought up to the reaction temperature in argon at atmospheric pressure and held for at least one hour. The pressure was then decreased to about 100 torr, and held for another hour. The pressure is given by Curve I in Fig. 3; somewhat lower pressures were frequently used without evidence of Si formation, indicating that the calculated P_I values may be high.

Temperatures were varied between 1650° to 1800°C without an apparent effect on yield and the ultimate particle size. However, high firing temperatures invariably gave better microstructures on hot-pressing. On firing at 1800°C, SiO_2 was fully reacted (no detectable SiO_2) and the yield of SiC was typically 80% of the theoretical based on the initial Si content. Powder blow-out, due to rapid gas evolution during the later reaction stages, is a continuing problem which, in small batches, could be overcome by decreasing the gas pressure slowly during these later reaction stages. On scaling up (15 lb batch) the fast onset of the reaction is still a major problem with this powder preparation process.

3.4.3 Decarburizing and Leaching

The excess carbon (about 15%) was removed by refiring of the calcinate at 700°C in air for several hours. Lower temperatures extended the time necessary and did not prevent oxygen pick-up which was about 2.5% (in one specimen analyzed) and presumably caused by surface oxidation. Decarburization was followed by leaching the powder in 25% HF for one hour, washing with 5% HF, with alcohol and drying at 120°C.

3.4.4 Powder Characterization

Selected powders were analyzed for metals, boron, nitrogen, oxygen, and carbon and by x-ray diffraction. Low temperature nitrogen adsorption was used to obtain surface areas. Two typical analyses are given in Table I. Determination of free silicon by two methods, gave differing results. Several percent of Si was found by leaching with HF + HNO_3[8] and none with KOH.[9] This discrepancy is not yet resolved. The indications obtained from sintering experiments are that some of the powders did contain small amounts of free silicon.

The described procedure yields yellowish β-SiC powders having stoichiometric composition and a specific surface area 10 to 15 m^2/g equivalent to 0.2 to 0.15 microns surface average crystallite diameter. The crystallites are heavily clustered into coherent aggregates (Fig. 4). Table II gives chemical analyses of three typical powders.

TABLE II

POWDER ANALYSES

Powder No.	Boron %	Nitrogen ppm	Oxygen %	Carbon %	Silicon %	C/Si
ES-3	0.46	40	0.59	29.05	69.15	0.982
ES-6	0.48	114	0.27	29.37	69.30	0.991
ES-11	0.46	--	0.40	29.10	69.25	0.988

4. PRESSURE-SINTERING AND MICROSTRUCTURE CONTROL

4.1 The Hot-Pressing Technique

Powder processing and the hot-pressing procedure described previously were used throughout the last period. Powder aggregate break-up by dry grinding with an addition of 1% of lubricant gave satisfactory materials for pressing. When additions of carbon were made, the powders were dispersed in a solution of an organic in benzene and the slurry was then dried or freeze-dried. Utilizing an isostatically prepressed pellet in the hot-pressing die instead of the loose powder yielded slightly better densities and die release of the final compact. This procedure was therefore used in most of the runs. The hot-pressing conditions were as follows;

Temperature - 1950°C (3540°F)
Pressure - 10,000 psi (6.085×10^7 N/m^2)
Time - 30 min

and were not altered unless the effect of the hot-pressing parameters were studied.

4.2 Results of Hot-Pressing

4.2.1 Fabrication Variables

The hot-pressing response of the powders prepared by SiO_2 reduction to 1% boron additions, temperature, ball-milling, specimen dimension etc.,

was in general similar to powder E277. However, three effects, which were related to prepressing, fluctuations of boron concentration and exaggerated grain growth and were not observed in the original experiments, complicated the response and sometimes obscured the results. These effects are discussed in turn below.

4.2.2 Boron Addition

An addition of 1% elemental B is necessary to achieve full densification at 2100°C (Table III). However, a boron addition made as H_3BO_3 on powder preparation is much more effective and 0.4% is sufficient to yield densities above 99.0%. Whether the difference in B effectiveness may be attributed solely to an improved distribution or whether there is a beneficial effect of boron on powder preparation is not presently known. Comparison of experiment Nos. R-37 and R-44 in Table III shows that an improved distribution of boron in the pre-pressing does have a strong effect.

4.2.3 Effect of Processing

Experiments Nos. 9, 10, and 11 in Table III demonstrate the effect of dry ball-milling on the final density. When milling was extended to 15 hours, wear of Carboloy balls was detectable (900 ppm tungsten). On wet-ball milling the ball wear was critical (approximately 1% tungsten in 16 hours) and this procedure was subsequently avoided.

4.2.4 Specimen Dimensions

Most specimens were 15g disks measuring 3/8" x 1". Variations in diameter (1" and 2") and length to diameter ratios (1/8 to 1) did not have a noticeable effect on final density (Table IV). Sectioning showed that the distribution of residual porosity was uniform with no indication of serious porosity gradients. As a result no difficulties are expected in further scaling up.

4.2.5 The Effect of Prepressing

The milled powders were prepressed into disks in a steel die at 10 Kpsi, repressed isostatically at 30 Kpsi and charged into the graphite die. Occasionally the preform cracked or was accidentally damaged and an investigation was made to determine if those materials were reusable. They were crushed to powder, sifted through a 40-mesh sieve, mixed with the remaining original powder, and repressed. The small fragments of the preform were strong and coherent, did not break down when pressed the second time, and resulted in bridging which prevented achieving uniform green density. The low density regions did not densify on subsequent hot-pressing because the high-density regions interlocked and halted the shrinkage process.

TABLE III

EFFECT OF SOME FABRICATION VARIABLES ON HOT-PRESSED DENSITY

No.	Exp. No.	Powder No.	Boron %	Temperature °C	Density g/cc	Relative Density %		
1	R-45	P-5	-0-	2100	2.33	73.0	Elemental Boron Added	
2	R-41	P-2	0.3	2100	2.69	83.9		
3	R-38	P-2	1.0	2100	3.24	100+		
4	R-37	P-2	1.0	1950	2.90	90.5		
5	R-44	P-5	1.0	1950	3.18	99.0		------15 hours ball-milling
6	R-69	ES-9	0.28	1950	2.91	90.9	Boron added on Powder Preparation as H_3BO_3	------Powder leached
7	R-42	P-6	0.4	1950	3.11	97.0		------Unleached
8	R-59	ES-3	0.46	1950	3.21	100		------Leached
9	R-46	P-7	0.4	1950	3.10	96.8		------Unmilled
10	R-47	P-7	0.4	1950	3.15	98.2		------Milled
11	R-48	P-7	0.4	1950	3.19	99.3		------Milled 16 hours
12	R-63B	ES-3	0.46	1950	3.06	95.5		------Repressed

TABLE IV

EFFECT OF SPECIMEN DIMENSIONS ON HOT-PRESSED DENSITY

Powder	Pressing Conditions			Dimensions (inches)		Density	
	°C	Kpsi	Min	Length	Dia.	g/cc	%
E-277	2100	10	50	1/8	1	3.22	100+
Same	2100	10	50	1/2	1	3.21	100
Same	2100	10	50	1	1	3.21	100
Same	2100	10	50	3/8	2	3.20	99.9
ES-14	1950	10	30	3/8	1	3.19	99.5
ES-14	1950	10	30	1	1	3.18+	99.3
ES-20	1950	10	30	3/8	2	3.17	99.0

This effect is demonstrated by Fig. 5 which shows fully dense islets within a porous matrix in the microstructure of pressing R-63B. It illustrates why only 95% relative density was achieved with a powder which yielded repeatedly theoretical density in prior experiments which were successfully conducted with a single prepressing step (e.g., R-59, R-63).

Similar effects have been observed on pressureless sintering of UO_2 and Al_2O_3[10, 11] but would not be expected in hot-pressing these materials, since macroscopic flow of a body under pressure should overcome the interlocking process. This is obviously not so in the case of SiC. Local variations in density are not removed during pressure sintering of such a material and consequently the conclusion was reached that processing to produce homogeneous green density is exceedingly important for the attainment of uniform shrinkage and compaction.

4.2.6 Boron Content Fluctuations

Most boron additions were made by adding boric acid during powder preparation equivalent to 0.5 w/o boron, based on the theoretical yield of SiC. Three powders initially analyzed showed that within experimental error (±0.05%B) the boron was reduced and retained in the SiC (0.38, 0.46, 0.48% B). All these preliminary powders sintered without difficulty to high density (>99%). Some powders produced later, however, failed to sinter satisfactorily but did show fine-grained microstructures (Fig. 6). Analysis of the boron content in these powders was rechecked with the results given in the following Table V.

TABLE V

POWDER ANALYSES

Powder No.	Boron	Oxygen	Hot-Pressing Density
ES-3	0.46%	0.59%	3.21 g/cc
ES-6	0.48	0.27	3.18
ES-9	0.28	0.32	2.91
ES-11	0.46	0.40	3.03
ES-14	0.40	0.20	3.06

At least in one case (Powder ES-9), the boron concentration of the above powders dropped below 0.3% and the decreased sinterability might well be attributed to this factor. When an additional 1% boron was added to this powder, it hot-pressed to the usual high density.

We conclude that the chosen batch boron addition, 0.5%, is too close to the limit of effectiveness, which is probably governed by the solubility limit of the boron in SiC under the hot-pressing conditions. When some boron is lost, due to evaporation, the residual boron content is not enough to bring about full densification and thus additions somewhat in excess of 0.5% are desirable.

4.2.7 Carbon Addition to SiC

Most of the powders made by reduction of SiO_2 showed exaggerated growth of tabular crystals on hot-pressing (Figs. 7 and 8). This anomalous grain growth could be detected before the final temperature and density were reached in specimens still exhibiting substantial porosity. Figure 9 shows tabular grains in powder ES-3 hot-pressed at 1900° to 90% density, i.e., 50°C below the sintering temperature. When this effect was more pronounced the fast growing grains impinged, interlocked, and stopped further densification and resulted in undesirably high residual porosities (Fig. 10). Such exaggerated grain growth was observed previously in hot-pressing powder E-277 at temperatures above 1950°C and linked to formation of a silicon phase.[1] A similar mechanism was suspected in the present case because a silicon phase could be frequently detected in the vicinity of the large grains (Fig. 11). Silicon was not necessarily present in the powder; it very likely formed from SiO_2 and SiC during hot-pressing.

To compensate for residual oxygen or silicon in SiC a 1% carbon addition was made to powders ES11 and 14 which showed the most extreme tabular grain growth and low final densities (Fig. 12).

Figure 13 shows the microstructure obtained and Table VI gives the density data:

TABLE VI

DENSITY-COMPOSITION CHARACTERISTICS

Exp. No.	Powder	Addition	Relative Density	Exagg. Grain Growth
R-72	ES-11	0.4%B	93.0%	Yes
R-74	ES-11	1.4%B	99.3%	Yes
R-75	ES-11	0.4%B+1%C	99.5%	No
R-82	ES-14	0.4%B	88.7%	Yes
R-81	ES-14	1%C+1.4%B	99.5%	No

The important conclusion from the above is that a small carbon addition can suppress exaggerated grain growth in SiC and generate fine grained bodies. This fact will be of unusual significance for the generation of SiC with desired high temperature mechanical properties.

4.3 Microstructure and Phase Composition

Three different types of microstructures were observed in hot-pressed, boron-doped submicron SiC.

A. Uniform 1-3μ equiaxed grains.

B. Large tabular crystals up to 500μ in 3-5μ matrix.

C. A uniform microstructure of 3-5μ elongated grains.

These three distinctly different microstructures can be discussed in terms of the total phase composition before and during hot pressing.

4.3.1 Microstructure Type A - 1-3μ Equiaxed Crystals

This morphology was obtained by hot-pressing SiC powders with relatively large contents of oxygen, such as Norton's E277 or powder obtained by the above procedure not leached with HF. The characteristics of the powders are in Table I (Columns 1 and 4) and those of the pressings in Table VII. The microstructures are shown in Figs. 14 and 15.

Only a fraction of the original oxygen (as SiO_2) remains in the SiC after hot-pressing. This silica was identified by selective etching of polished sections with HF (5% for 6 sec; see Fig. 16), by TEM and electron diffraction

TABLE VII

CHARACTERISTICS OF HOT-PRESSED SPECIMENS

Sample No.	R-30	R-42	R-48	R-63	R-75
Hot-Pressing Conditions	1950°C 10 Kpsi 30 min	Same	Same	Same	Same
Starting Powder	E-277<1μ	ES-2	P-7	ES-3 (leached)	ES-11
Density, g/cc	3.19	3.15	3.18	3.20	3.20
Grain size, microns	3.2	0.4	4.8	3.8 (matrix)	3.0
Largest observed grains, microns	~10	2.0	40	>500	25
Phases detected	βSiC αSiC SiO_2	βSiC SiO_2	βSiC αSiC Si	βSiC αSiC Si + unknown	βSiC C
Chemical Composition:					
Boron, %	0.88	0.42	0.40	0.40	0.46
Oxygen, %	0.54	2.2	0.048	0.087	<0.006
Total metal impurities (mainly Fe, Al, Ti, Zr, V)	<0.4	--	<0.2	--	--

(Fig. 17). Detailed observations of these micrographs revealed that SiO_2 is distributed along SiC grain edges but does not form a continous grain boundary phase. SiO_2 should have a small but non-zero wetting angle (<45°) in contact with SiC. The revealed "grains" in Fig. 16 are in fact sections through the channel-like network of SiO_2. There are also two or three whole loops around SiC grains. It is likely that this phase was a viscous melt at the forming temperature and controlled grain growth during hot-pressing and gave rise to a grain shape typical for relatively slow, normal grain growth.

TEM shows a high density of stacking faults and twinning which is probably typical for hot-pressed SiC.[12] This was also revealed by thermal etching in Fig. 15. No additional phases could be detected besides the SiO_2 and an insignificant number of shiny grains, probably silicon, that were observed optically.

4.3.2 Microstructure Type B - Large Tabular Crystals in a 3-5μ Fine-Grained Matrix

This type of microstructure is shown in Figs. 7 and 8. There are marked variations in tabular morphology as shown in Fig. 18 which demonstrates a moderate case, and in Fig. 12, which demonstrates an extreme case. Ultimately, all the matrix may transform into the large tabular grains. X-ray and electron diffraction identified the matrix as β-SiC and the tabular grains as α-SiC-6H (Table VII), implying that exaggerated grain growth involves a phase transformation. Besides these two phases, a small amount of a free silicon phase is always found, as shiny grains, in the as-polished sections (Fig. 11) or trapped inside pores. The volume fraction of this phase is very small, certainly less than 1%.

The study of thin sections revealed that the large α grains are transparent and colorless which is an appearance typical for this phase.[13] Pores trapped within and at the boundaries of grains are partly filled with a dark-brown, optically isotropic phase which is obviously a melt at the sintering conditions. This phase was not identified; however, microprobe analysis showed it to have a variable silicon to carbon ratio and traces of Fe, V, and Al impurities.

4.3.3 Microstructure Type C - 3-5μ Elongated Grains

A small addition of carbon, typically 1%, to the synthesized powders suppresses the exaggerated grain growth shown in Type B microstructures (Fig. 13). The black spots in this micrograph are carbon grains resulting from inhomogenieties of the carbon distribution in the powder.

Microstructures containing large but equiaxed grains in a fine-grained matrix were also observed (Fig. 19). The large grains were β-SiC and were frequently twinned. They resemble microstructures obtained by Nadeau[1] on high-pressure hot-pressing of SiC. In a few cases, the grain-growth-inhibiting effect was localized around the surface of the hot-pressed billet with the gross tabular grain growth occurring only in the core of the pressing (Fig. 20). The microstructure around the surface was very similar to that shown in Fig. 13.

Type C silicon carbide was β-phase and exhibited no secondary phases other than a very small amount of residual carbon. Chemical analysis showed a very low oxygen content (0.005%-Table VII).

4.4 Discussion

Exaggerated grain growth (EGG) was a critical problem in the recent study because large grains were strength limited (See Chapter 5, para. 5.3). Although the technique of carbon addition was found to suppress it, a future understanding of this phenomenon is highly desirable to prevent unexpected failures due to poor microstructure development.

Exaggerated grain growth has frequently been observed in ceramics, such as ferrites and alumina and has been attributed to the presence of a small amount of a melt having an appreciable solubility for the main constituent. Stuijts[14] concluded that a liquid growth mechanism promotes EGG in ferrites as he observed right-angle intersections of the matrix grain boundaries with the boundaries of larger grains. Besides the presence of the liquid, a small nucleation frequency is obviously a necessary condition for the phenomenon to occur.

The observations made about EGG in SiC are summarized in the following:

1. EGG was observed above 1800°C in all stages of densification; i.e., in fully dense body as well as in a loose powder.

2. Small amounts of silicon are frequently found in the vicinity of the large grains. However, a 1% silicon addition to SiC does not induce EGG.

3. Small amounts of oxygen, a few tenths of a percent, were typical for powders exhibiting EGG. Bodies with suppressed EGG had lower oxygen contents.

4. EGG was also observed on pressureless annealing of the pressings having A-type microstructure at temperatures equal to or above the sintering temperature.

5. There were two distinct morphologies of the tabular grains:

   a. Thin, very large plates, up to several milimeters long, with an aspect ratio up to 100, growing in dense bodies (Fig. 12).

   b. Smaller and thicker plates with an aspect ratio of about 10, which grow at early stages of densification in porous compacts and in loose powders (Figs. 7 and 8).

6. The large crystals are invariably α-SiC and grow from a β-SiC matrix or β-SiC powder. They are mostly transparent and colorless.

7. A brown phase, apparently a solidified melt, is frequently found trapped in pores.

The experimental observations led us to conclude two transport mechanisms. In the early stages of densification (porous compacts) a liquid transport mechanism is unlikely and hence vapor transport is likely. In dense specimens, a vapor transport is impossible and a dissolution-reprecipitation process is likely to be responsible.

The partial pressures of SiC, Si_2C, and SiC_2 below 2000°C are too low to be important and another volatile substance must be considered. The observed presence of oxygen suggests that the cycle proposed by Dietzel[7] may be operative:

$$SiC_{(s)} + SiO_{(g)} \rightleftarrows 2\ Si_{(\ell)} + CO_{(g)} \qquad (4.1)$$

$$Si_{(\ell)} \rightleftarrows Si_{(g)} \qquad (4.2)$$

The free energy of reaction (4.1) at 1900, 1 atm and $P_{SiO}/P_{CO} = 1$ is only 500 cal so that it may be reversed by local variations of Si vapor pressure (due to grain size) or by the difference in energy content between the β and α phases. The process is essentially a vapor-liquid-solid (VLS) growth mechanism and it is understandable that it may be extremely fast where the reacting and growing species are only fractions of a micron apart. The well-developed crystalline habit of some SiC plates formed in loose SiC powders on heating above 1800°C is strong support for the occurrence of the vapor transport mechanism.

The EGG mechanism operating in a dense polycrystalline body requires a liquid phase with a melting point near 1900°C that has an appreciable solubility for SiC. Originally, silicon formed by the following reaction (4.3).

$$SiO_{2(\ell)} + 2SiC_{(s)} = 3\ Si_{(\ell)} + 2CO_{(g)} \qquad (4.3)$$

was considered. However, two observations indicate this reaction to be highly unlikely. Firstly, silicon additions to fine-grained SiC do not induce EGG (though they retard densification) and, secondly, reaction 4.3 would be controlled by CO diffusion through SiC and therefore would be a very slow process. After annealing a piece of Type A SiC at 2100°C, EGG was observed after 30 minutes uniformly throughout a 1/2" x 1/2" cylinder. Moreover, reaction (4.3) does not proceed at high pressures according to the calculated phase equilibria (Fig. 2) but instead, reaction (4.4), as follows, should occur and yield silicon monoxide. It is tentatively suggested that

$$SiC_{(s)} + SiO_{2(\ell)} = C_{(s)} + 2SiO_{(c)} \qquad (4.4)$$

condensed silicon monoxide is the phase responsible for EGG.

The existence of solid SiO is controversial at low temperatures but at high temperatures, its existence seems to be well established.[15] Its melting point was estimated to be above 1700°C and on cooling to temperatures below 1200°C, SiO disproportionates into a mixture of Si and SiO_2.

The effect of carbon in suppressing EGG may be understood in terms of the following proposed mechanism. Carbon probably removes residual oxygen during heating. When time is not given for the reduction of SiO_2 to be completed

and CO to escape, then pores will close and reaction (4.4) will take over at some temperature above 1800°C and trigger EGG. This may explain the exaggerated grain growth behavior which is localized in the core of a pressing as shown in Fig. 20.

It is interesting to note that the β to α SiC transition observed in our experiments has been controversial for many years. Our work suggests that this transformation is thermodynamically preferred below 2000°C but is dependent on the availability of a suitable transport mechanism.

5. MECHANICAL PROPERTIES TESTING

5.1 Procedures

Mechanical properties measurements have provided data for the comparison of processing and microstructure limiting parameters with actual material strength. This, in turn, has provided feedback information to promote further SiC development. Less elaborate, readily available procedures, such as three point bending in creep and strength evaluation were preferred. The temperature of testing was increased to 1620°C to fully cover the temperature region of future interest. Creep at this upper temperature for some of the materials was nearly undetectable and thus the measurement accuracy is limited. Results, however, do illustrate the differences between the three types of microstructures discussed above.

5.2 Flexural Strength

Hot-pressed SiC specimens were cut from identical 1"-diameter billets into test bars 0.1" x 0.1" x 1.0" and machined with a 200 mesh diamond wheel. The two longitudinal edges to be in tension were smoothly chamfered and specimens with major defects detectable in a 5X magnifying binocular were discarded. Tests were run in three point bending on a 0.625" span at 0.002"/min traverse speed at room temperature, 1300°, 1400°, and 1500°C using an Instron machine. Tests at 1600°C were made on 0.05" x 0.1" x 1.0" bars on a 0.75" span in the test rig built for creep measurements. The materials selected have been characterized in Table VII and include:

R-30, Type A - containing SiO_2

R-63, Type B - containing isolated large tabular grains of α-SiC and free silicon

R-90, Type C - containing carbon.

The results are listed in Table VIII and Fig. 21. Also included is data obtained formerly on material R-30.

The two fine-grained silicon carbides, R-30 and R-90, retain a strength of about 80,000 psi up to 1400° and 1500°C, respectively, and both show a

TABLE VIII

FLEXURAL STRENGTH OF HOT-PRESSED SiC, PSI

Temperature / Specimen	Room Temp.	1300	1400	1500	1600
R-30	82,000 (12)	78,900 (7)	78,200 (7)	67,800 (7)	44,000 (4)
R-63	39,000 (5)	38,700 (5)	37,500 (5)	36,600 (5)	------
R-90	71,900 (10)	80,000 (5)	81,900 (4)	84,100 (5)	63,700 (6)
R-30 (1971)	80,200 (2)	-----	-----	-----	-----
R-30 (1971) (polished)	103,200 (4)	-----	-----	64,000 (4)	-----

See Table VII for characterization.

Note: Number of specimens given in parentheses.

remarkable strength even at 1600°C. The faster drop in strength of SiC R-30 is attributed to its silica content and resulting effect on slow crack propagation. The oxygen-free material showed an increase in strength from 71,000 psi to 84,000 psi over the same temperature range. A strength increase in SiC with temperature was also reported by Alliegro[16] and for CVD SiC by Gulden[4]. In the present case, however, it is uncertain whether it is a real phenomenon. It may be related to the yielding of the alumina support pins, which is sufficiently large to improve aligning and reduce twist. The noticeable decrease in scatter above 1300°C is also attributed to this yielding effect.

Type A and C specimens showed small differences in strength and were fabricated and machined as described previously. Also, both specimen types had a maximum grain size well below the size of the estimated flaw size necessary to initiate fracture. It is concluded that their strength was probably controlled by similar stress concentrators resulting from surface damage introduced by machining. This is supported by the increase of room temperature strength measured on polished and lapped test bars. The absence of polishing effects on the 1500°C strength may be attributed to a change in fracture mechanism at this temperature.

5.3 Flexural Strength - Material R-63

The R-63 SiC was dense (99.5%) but contained isolated, randomly distributed large grains, up to several hundred microns (Figs. 7,8) and this structure suggested the possibility of a unique series of experiments. The objective of these experiments was to determine whether or not large grains in a fine-grained matrix would act as inherent flaws and would consistently initiate fracture. This effect is expected due to the lower fracture energy of single crystals compared to polycrystalline solids. Straightforward evidence on this point has not been available and, in addition, if such proved to be the case then important information on the geometries and sizes of fracture nucleating flaws could be obtained.

The strength measurements were made as described previously and the results are summarized in Table IX. The fracture surfaces were investigated and, in the majority of cases, fracture initiation was clearly localized at the large crystals intersecting the tensile face of the specimen. In two cases, there was fracture initiation at large interior grains and in four cases, the origin was uncertain. (While the grains initiating fracture were identified no clear evidence on the direction of fracture propagation was obtained.) Table IX lists the strength results in relation to the sizes of these identified grains. Comparing matching pairs of specimen fragments showed that fracture propagated through the bulk of the large crystals and avoided the path along the crystal-matrix boundary.

The data in Table IX gives the largest dimension of the isolated crystal to which fracture initiation was attributed. These crystals were observable

TABLE IX

SIZE OF GRAINS INITIATING FRACTURE

Spec. No.	Temp. °C	Strength KPSI	Maximum Dimension of Grain Initiating Fracture, μ	
8987	Room Temp.	50.4	(230)**	
8988	"	36.6	495	310
8989	"	44.0	315	
8991	"	40.2	(290)	
8992	"	23.8	990	
8993	1300	34.2	415	
8994	"	26.2	1680	1090
8995	"	47.0	155	
8996	"	52.0	(175	63)
8997	"	32.0	670	400
8998	1400	53.5	145	
8999	"	31.8	930	740
9000	"	25.9	1250	
9001	"	28.5	1300	800
9002	"	48.0	250*	
9003	1500	33.8	730	390
9004	"	36.8	640	500
9005	"	46.0	(400)	
9006	"	28.7	1140*	
9007	"	37.8	720	

*Fracture initiated at internal grain.

**Numbers in parentheses refers to fracture surfaces which did not reveal the direction of fracture propagation.

in the fracture surface using a microscope with an extra-long focus objective. These measurements were, however, somewhat ambiguous in that two fragments of one test piece usually did not yield precisely the same length. Therefore, two measurements are given whenever this difference was larger than 20%. The larger value was used, however, in plotting strength vs the inverse square root of the size of the crystal in Fig. 22.

The relation obtained in Fig. 22 has the form of the Petch equation[17]

$$\sigma_f = \sigma_o + K(GS)^{-1/2} \qquad (5.1)$$

where σ_f = fracture stress
GS = size of grain initiating fracture
σ_o, K = constants

and shows that the large grains affect strength as if they were cracks. This is justified by the following consideration.

The difference in elastic constants of the β-SiC matrix and the α-SiC crystal will cause stress concentrations which are, according to Hasselman[18],

$$\sigma = \frac{E_\alpha}{E_\beta}\ \sigma_a \qquad (5.2)$$

σ = effective stress

σ_a = applied stress

E_α = Young's modulus of α-SiC phase

E_β = Young's modulus of β phase

This relation, applied to our SiC results, assumes a large length to thickness ratio of the inclusion of the isolated α-SiC crystal. Numerically, the stress concentration factor, E_α/E_β, about 1.65.

The magnified local stress, σ, operates at a flaw within the stress field of the isolated crystal and will propagate a crack across the grain which has a surface fracture energy 5 to 10 times less than the matrix[19]. The crack will be arrested at the boundary of the crystal where fracture energy abruptly increases and the stress field generated by elastic stress concentration vanishes.

When the data of Fig. 22 are extrapolated, one can estimate the size of the strength-limiting defects in the series of measurements on material which exhibited 80 Kpsi fracture strengths (Fig. 23). The extrapolated flow size for this material is 45μ, which is a value much greater than the largest observed grain in these fine-grained specimens. Hence, one infers that fracture is initiated in these high-strength materials by extrinsic defects. The same conclusion was arrived at by Lange[20] for the strength of dense, fine-grained silicon nitride.

The diagram in Fig. 22 was plotted on the a priori assumption of the validity of the inverse square root relationship between fracture stress and crack length (i.e., the Griffith equation) and brings about the problem of accounting for the intercept, σ_o, which extrapolates to 17 Kpsi at infinite crack length. This is a controversial point well known from studies of grain size dependence of strength in brittle solids.[21-23] In this case, however, the value of σ_o is far too low to be related to yielding[24] and another explanation should be sought.

There are important implications of this result. Firstly, in assessing microstructures in relation to strength, attention must be paid mainly to the

largest structural features (grains, pores, inclusions, etc.) no matter how infrequently they occur. This is a difficult analytical problem, but it does show the need for the full development of extreme value statistics for application to fracture mechanics in brittle materials. Secondly, strength improvement should be obtained by elimination of fairly large defects, not yet identified before the intrinsic strength limitation imposed by maximum grain size is reached. It is believed that this may be achieved by perfection of processing and elimination of surface damage due to machining. This will be a most important step in fabrication of these materials.

5.4 Creep Measurement

Data available on creep and diffusion in SiC[25-29] predict strain rates of the order of 10^{-6} to 10^{-9} per sec at 1600°C. These strain rates are measurable at constant stress but, at the low limit, require long-time experiments.

A test apparatus for creep measurements in air up to 1650°C was assembled on a standard frame with a platinum-40% rhodium wound furnace and concentric silicon carbide grips as schematically shown in Fig. 24. The grips were made of KT-SiC which was fired at 2000°C in argon prior to machining and are mounted in a water-cooled extension tube and rod. The deflection transferred by the central rod was detected by an LVDT (linear variable differential transformer) amplified and recorded. There is no limitation to amplification but noise, outside thermal fluctuation, and other effects limit useful sensitivity to about 100μ scale reading. Thus, in the current apparatus, it is possible to detect a 1μ deflection and a minimum strain rate of about 5×10^{-10}/sec. Temperature is measured by two calibrated Pt 6Rh/Pt 30 Rh thermocouples and controlled by an on-off capacitance controller within ±3°C. The variations are mainly affected by ambient and cooling water temperature fluctuations and are subject to improvement. Load is imposed by a calibrated spring balance and the smallest load is determined by the weight of the push rod; i.e., 390g. Specimens are 0.05" x 0.1" x 1.0" machined bars.

A typical run takes several days when stress or temperature dependence of strain rate is to be evaluated. There is always observed an initial transient creep attributed to several processes of which three were identified: aligning of the specimen with the knife edges and the pin, indentation at the contact lines, and a true transient creep. We were interested in steady creep which indeed is achieved (within the precision of our measurements) in several hours at stresses about 25,000 psi.

The total deflections were small, up to 50 microns, and the simplied relation

$$\varepsilon = \frac{4hd}{s^2} \qquad (5.3)$$

ϵ = strain

h = height of specimen

d = deflection

s = span

was appropriate to evaluate the strain.

Creep of three previously characterized materials (Table VII) was measured and evaluated as strain rate per second in Table X and plotted as strain rate vs stress in Fig 25 and vs inverse temperature in Fig. 26.

The log strain rate-log stress dependence has a slope 1.2 and makes the applicability of diffusion models uncertain. Therefore, the evaluation of diffusion coefficients was not attempted at this stage. To obtain some comparison with earlier work, we plotted in Fig. 27 data obtained by Francis and Coble[26] for creep of a dense SiC having a 9.5μ grain size. (The data were converted to the nominal stress 25,000 psi used in plotting Fig. 26.) Though the activation energies are markedly different, it is interesting to observe that the extrapolated data of strain rate of our specimen R-48 coincide with the location of the data quoted. The values of strain rate for R-30 and R-81 (Type A and C microstructures) are close, within experimental error, and one concludes that small amounts of SiO_2 in SiC, about 1%, do not affect high temperature deformation behavior. This is understandable as SiO_2 was found distributed along grain edges and does not form a boundary layer.

Specimen R-48 shows a creep rate an order of magnitude higher than R-30 and R-81 though it has a larger grain size (Table VII). A 1% carbon addition was used in preparation of specimen R-81 and had clearly a highly beneficial effect on creep resistance. It was speculated that the increased creep rate of specimen R-48 was linked to its small content of free silicon; i.e., to the stoichiometric excess of Si with might be, in turn, reflected in carbon vacancy concentration. Carbon is known to be the slower diffusing species in SiC and a carbon vacancy diffusion mechanism was proposed by Ghoshtagore.[24] Such a model would, of course, also account for the reverse effect of carbon.

The results on creep are preliminary and need to be extended to higher temperatures and to different grain sizes to develop insight into the creep mechanism in SiC. This is a major task and some work in this direction has been planned. Nevertheless, the pronounced effect of minor compositional changes is a critical piece of information. It should be realized that the creep rate observed is by no means negligible. The higher value for instance (1.2×10^{-8}/sec at 1600°C and 25,000 psi) is equivalent to a deformation of 15% a year at 10,000 psi.

Table X

SUMMARY ON CREEP EXPERIMENTS

Material (See Table VII)	Temperature °C ± 3	Stress PSI	Strain Rate $\dot{\varepsilon}$/sec
R-30	1614	22,000	1.90×10^{-9}
	1614	27,500	2.6×10^{-9}
	1614	32,000	3.4×10^{-9}
R-30	1619	27,500	2.0×10^{-9}
	1640	27,500	3.9×10^{-9}
	1662	27,500	6.35×10^{-9}
R-48	1603	27,500	6.2×10^{-9}
		32,000	1.3×10^{-8}
R-48	1614	7,700	0.43×10^{-8}
	1614	22,400	1.0×10^{-8}
	1614	27,600	1.5×10^{-8}
	1614	32,400	2.0×10^{-8}
R-81*	1660	27,500	1.2×10^{-8}
	1642	27,500	4.0×10^{-9}
	1620	27,500	3.1×10^{-9}
	1622	41,000	5.6×10^{-9}
	1622	50,900	7.4×10^{-9}

*R-81 is identical in composition and microstructure to R-75. (See Table VII.)

TABLE XI

SUMMARY OF DATA ON DELAYED FRACTURE

Exp. No.	Specimen No.	Kpsi	% of Strength	Time to Fracture	Time of Experiment (mins)
1	R-30	25	57	---	4200
2		25	57	---	4200
3		25	57	---	4200
4		30	68	405	405
5		30	68	---	4200
6		30	68	---	4200
7		35	80	65	65
8		35	80	21	21
9		40	91	3	3
10		40	91	2	2
11	R-81	50	78	---	3000
12		50	78	---	2900
13		60	94	2	2
14		60	94	12	12

5.5 Delayed Fracture

Creep tests in bending of SiC conducted at temperatures of 1600°C and stresses of 30,000 psi and higher also yielded delayed fracture data. Ten measurements for material R-30 (SiO_2 containing) and four for R-90 (carbon containing) have been made. The data is listed in Table XI and plotted in Fig. 28 as fracture stress vs log time. We included further data of fracture strength measured at the same temperature in a loading cycle of about 40 to 50 seconds (four data points).

The results suggest that there is a slow crack growth in SiC at 1600°C under stresses above 60% of the fracture stresses measured in normal, quick loading, flexural tests. The slow crack growth was indeed observable in a few cases. The design of the grips allows the fragments of the test bars to fall down along the push rod out of the hot zone and to be quenched from 1600°C to room temperature. Unfortunately, it is not controllable and in many cases,

the fragments adhere to the obviously soft sticky oxide layer on the grips. However, when the quench does happen after a long exposure at 1600°C the slow growing crack may be traced in the fracture surface because it has different texture and color due to oxidation. One of the two well discernible "slow" cracks is shown in Fig. 29. The maximum length of the two observed cracks was measured and identified with the crack length at catastrophic failure and the results are given in Table XII.

TABLE XII

STRENGTH AND FLAW SIZE OF SiC R-30

Exp. No.	Temp. °C	Stress at Fracture (Kpsi)	Crack Length (mm)	Fracture Energy (erg/cm^2)
CD 502/72	1591	40	0.185	22,200
CD 504/72	1595	40	0 205	24,500

From these crack lengths the fracture energy was calculated according to the following relation proposed for "penny-shaped" cracks by Sack.[19]

$$\sigma_f = \left[\frac{\pi E \gamma_f}{2C(1-\nu^2)} \right]^{1/2} \qquad (5\text{-}4)$$

where:

E is Young's Modulus

ν Poisson's ratio

C Crack length

The two values of fracture energy in Table XII agree satisfactorily with that obtained in the previous experiment at lower temperatures.

The important conclusion is that there is slow crack growth in SiC under stress at high temperatures and the investigation of its kinetics and mechanism is an important and necessary adjunct to the study of this class of materials.

6.0 OXIDATION OF HOT-PRESSED SiC

Qualitative tests of stability of hot-pressed dense SiC at 1400° and 1600°C in air were reported and discussed previously.[1] In this period, we have compared the oxidation behavior of two fine-grained hot-pressed SiC materials (silica containing specimen R-30 and an oxygen-free specimen R-63) with CVD SiC as a reference material.* We also evaluated one commercial hot-pressed silicon carbide material.

*The CVD SiC was a fine-grained (submicron) material prepared by J. Diefendorf at RPI in 1972.

Experiments were run in a muffled moly-wound furnace in a slow air stream. The specimens were wafers about 3/8" x 3/8" x 0.05" as cut by a diamond wheel. They rested on SiC single crystals on an SiC pedestal. This arrangement eliminated undesirable chemical interactions. At long exposures, minor sticking could not be prevented, however, and may have introduced some small errors. After selected periods of time, the specimens were weighed on a microbalance with an accuracy of ±0.02 mg. Table XIII lists the weight gains per cm^2 of surface area and Fig. 30 is a plot of weight gain vs square root of time.

The weight gains correspond to silica surface layers 5.0, 6.7, and 20 microns thick for the CVD, R-30, and R-63 SiC, respectively. The commercial SiC was not evaluated because of heavy bloating of its surface layers as shown on Fig. 31. This bloating is most likely caused by metallic impurities in this material which decrease the viscosity of the silica surface layer.

The curves in Fig. 30 have two branches: the initial period during which oxidation proceeded at a relatively fast rate corresponds perhaps to the build-up of the oxidation layer on the rough surface and filling in small dents and crevices by SiO_2. After this has been accomplished, diffusion controlled oxidation is expected to take over. In our experiments, the oxidation rate in this second period was too low to allow evaluation of the diffusion coefficients.

TABLE XIII

OXIDATION OF SILICON CARBIDE AT 1600°C

Specimen	CVD-SiC	R-30	R-63	Commercial Dense
Total Time of Exposure Hours	Weight Gain mg/cm^2 at 1600°C			
0.5	0.12	0,18	0.23	3.33
1.0	0.34	0.27	0.45	4.86
2.0	0.41	0.37	0.74	6.70
4.0	0.41	0.40	0.95	4.90
8.0	0.44	0.53	1.35	1.41
14.0	0.39	0.55	1.49	-4.26
32.0	0.37	0.52	.54	-9.90
57.0	---	0.53	1.56	-20.20

The larger weight gain of specimen R-63 at the time of the onset of the steady state oxidation period was linked to recrystallization of the silica layer on this specimen. It may be seen in Fig. 31 that during the exposure, there formed white milky areas in its surface. These areas had a clearly crystalline appearance in the microscope and probably contained cristobalite.

The excellent oxidation resistance of the boron-doped hot-pressed SiC previously reported was confirmed in two other materials and compared with a boron-free fine-grained CVD-SiC. There is clearly no detrimental effect of the small amounts of boron on high-temperature stability in air.

REFERENCES

1. S. Prochazka, "Investigation of Ceramics for Turbine Vanes," Final Report, SRD-72-035, 1972.

2. M. L. Torti, "Materials Development Si_3N_4, ZrB_2-SiC," Nineteenth Meeting of the Refractory Composite Working Group, Houston, 1972.

3. G. Q. Weaver and B. A. Olson, "High Strength Silicon Carbide," Si_3N_4 and SiC Symposium, May 1972, Washington, D. C.

4. T. D. Gulden, "Mechanical Properties of β-SiC," J. Am. Ceram. Soc., 52, 591 (1969).

5. D. P. H. Hasselman and H. D. Batha, "Strength of SiC Single Crystals," Applied Phys. Letters 2, 111 (1963).

6. W. A. Krivsky and Schuhmann, "Derivation of Phase Diagram for the Si-O-C System," Trans. AIME 221, 898 (1961).

7. W. Poch and A. Dietzel, "Die Bildung von SiC aus Si und C," Ber. D. K. G. 39, 413 (1962).

8. G. Serrini and W. Leyendecker, "Determinazione a livello semimicro. . . . ," Metall. Ital. 4, 129 (1972).

9. Chemische Analyse von SiC, DIN. 51075.

10. C. Majani et al., "Some Pressing, Kinetic, and Structural Parameters of UO_2," Phys. Sint. 1 (1969), M1.

11. T. Vasilos and W. Rhodes, "Fine Particulates to Ultrafine-grain Ceramics," in Ultrafine-Grain Ceramics, J. J. Burke, Ed., 1970.

12. R. Stevens, "Defects in Silicon Carbide," J. Mat. Sci. 7, 517 (1972).

13. P. T. B. Shaffer in "Silicon Carbide," H. K. Henish, Ed., p. S97, 1969.

14. A. L. Stuijts and C. Kooy, "Influence of Technological Factors in the Sintering Behavior of a Ferrite," in Science of Ceramics, Vol. 2, G. M. Stewart, Ed., 1956.

15. L. Brewer and R. K. Edwards, "The Stability of SiO Solid and Gas," J. Phys. Chem. 58, 351 (1959).

16. R. A. Alliegro, L. B. Coffin, Jr., and J. R. Tinklepaugh, "Pressure-Sintered Silicon Carbide, J. Am. Ceram. Soc., 39, 386 (1956).

17. N.J. Petch, "Cleavage Strength of Polycrystals," J. Iron Steel Inst. London, 174, 25 (1953).

18. D.P.H. Hasselman, "Single Crystal Elastic Anisotropy and the Mechanical Behavior of Polycrystalline Materials," in "Anisotropy of Single Crystals," W. Vahldiek, Ed., 1968.

19. R.W. Davidge and A.G. Evans, "The Strength of Ceramic," Material Sci. Eng., 6, 281 (1970).

20. F.F. Lange and G.R. Terwilliger, "Fabrication and Properties of Silicon Compounds," Final Report NASC N00019-71-C-0107, 1971.

21. S.C. Carniglia, "Re-examination of Experimental Strength vs Grain-size Data for Ceramics," J. Am. Ceram. Soc., 55, 243 (1972).

22. F.P. Knudsen, "Dependence of Mechanical Strength of Brittle Polycrystalline Specimens on Porosity and Grain Size," J. Am. Ceram. Soc., 42, 376 (1959).

23. S.C. Carniglia, "Petch Relation in Single-Phase Oxide Ceramics," J. Am. Ceram. Soc., 48, 580 (1965).

24. R.W. Rice, "Strength Grain-size Effects in Ceramics," Proc. Brit. Ceram. Soc., 20 (1972), 205.

25. R.N. Ghoshtagore and R.L. Coble, "Self-Diffusion in Silicon Carbide," Phys. Rev. 143, 623 (1966).

26. T.L. Francis and R.L. Coble, "Creep of Polycrystalline SiC," J. Am. Ceram. Soc. 51, 193 (1969).

27. P.L. Farnsworth and R.L. Coble, "Deformation Behavior of Dense Polycrystalline SiC," J. Am. Ceram. Soc. 49 (1965), 269.

28. P. Marshal and R.B. Jones, "Creep of Silicon Carbide," Powder Met. 12 (1969), 193.

29. J.C.V. Rumsey and A.L. Roberts, "Delayed Fracture and Creep in Silicon Carbide," Proc. Brit. Ceram. Soc. 17 (1970), 233.

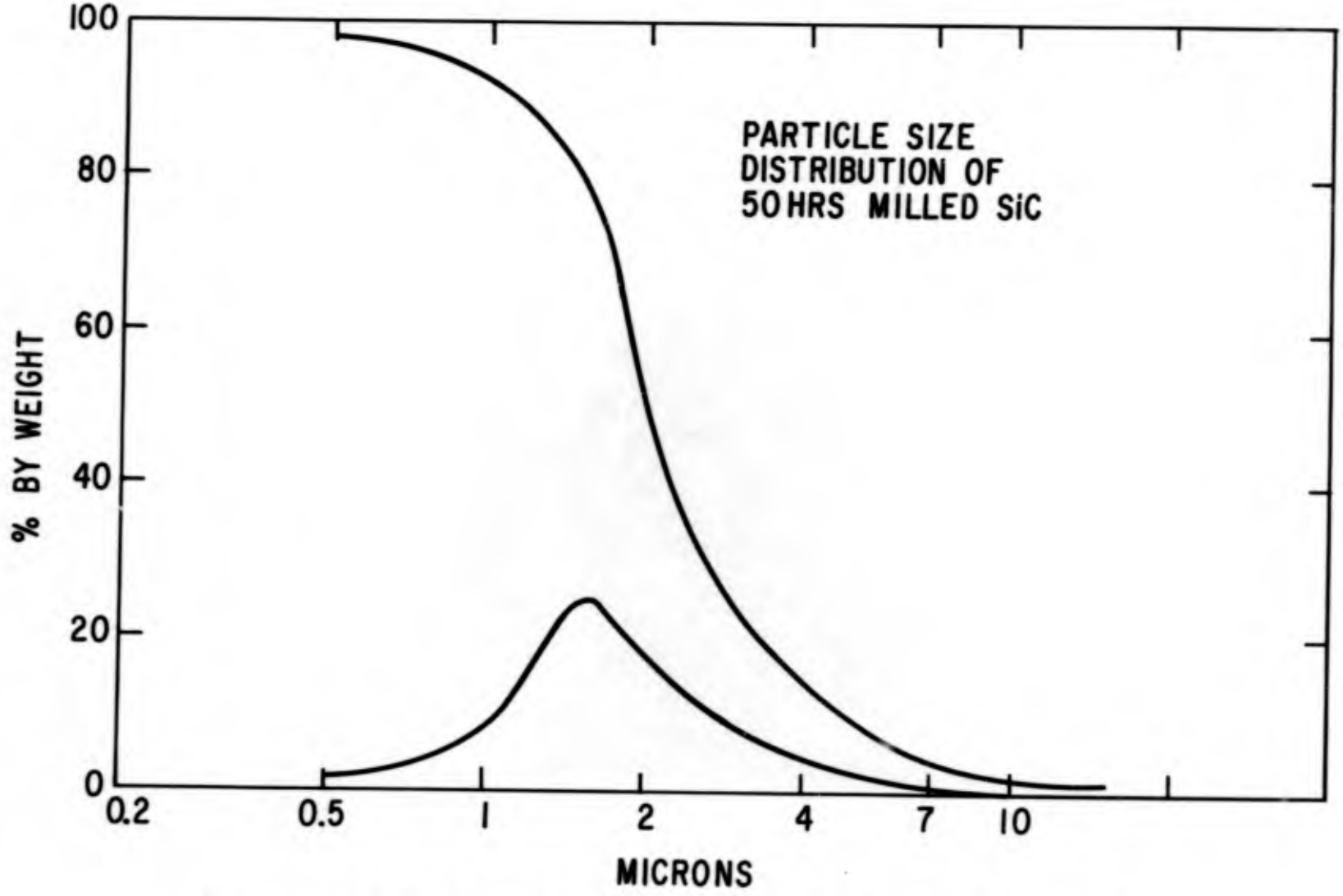

Fig. 1 - Particle size distribution of 600 mesh SiC, milled 50 hours. Coulter Counter.

Fig. 2 - Morphology of silicon carbide particles formed from silicon and carbon at 1500°C in argon; X10,000.

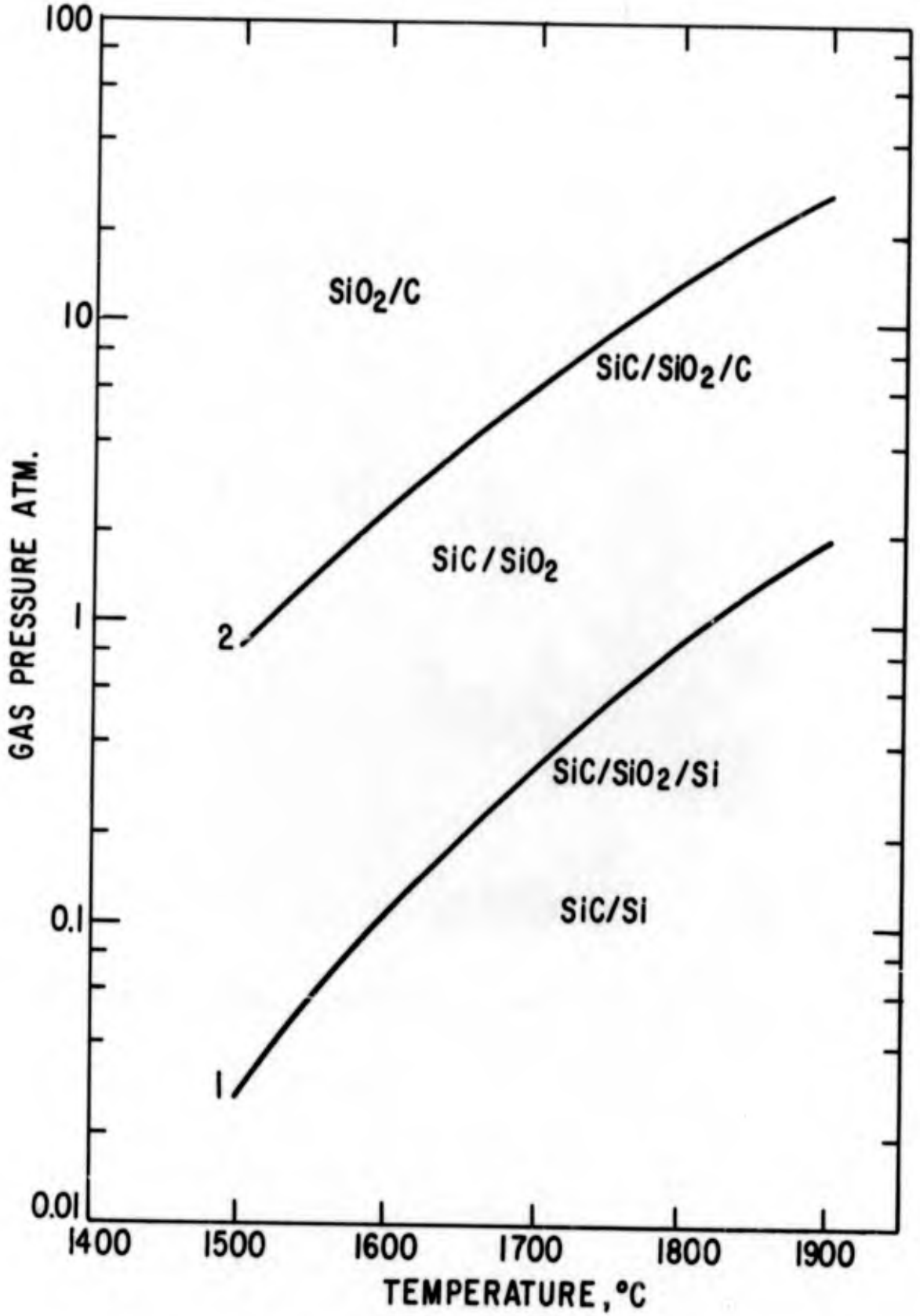

Fig. 3 - Temperature-gas pressure relation in the Si-C-O system.

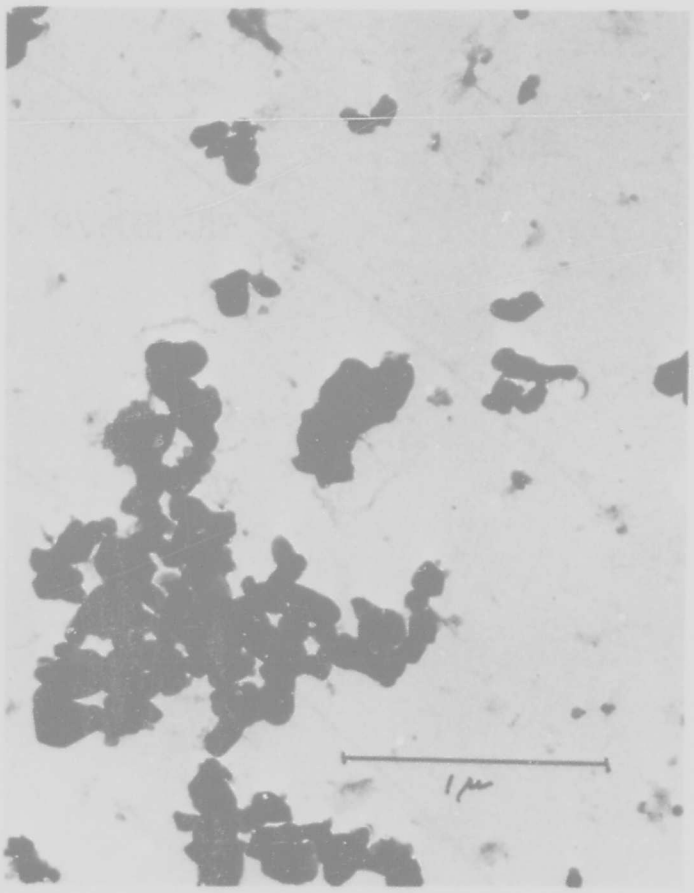

Fig. 4 - Morphology of silicon carbide formed by reduction of amorphous silica. 30,000X.

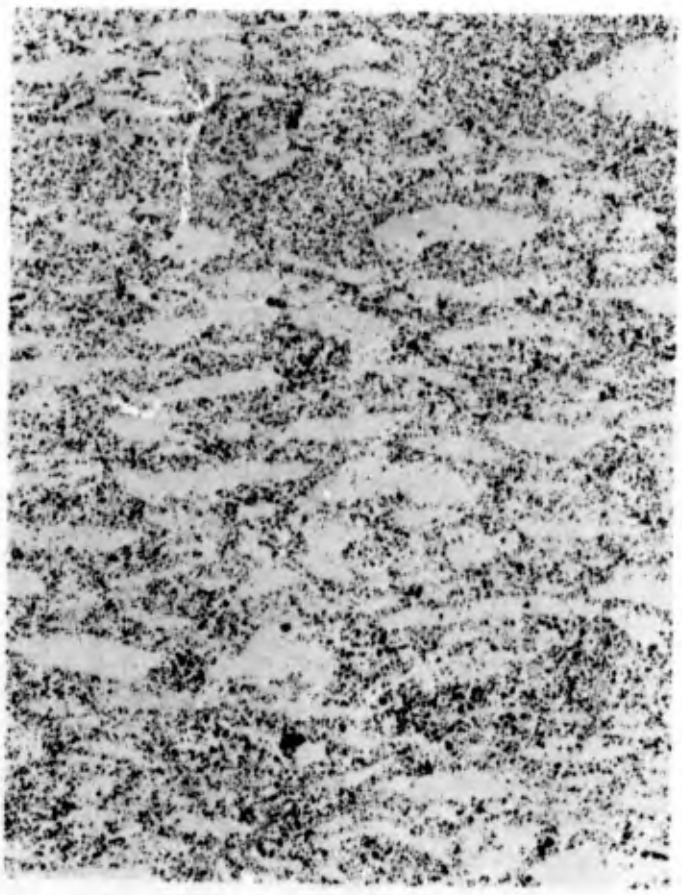

Fig. 5 - SiC R-63B. As polished, 100X. Density variations caused by unhomogenious pressing powder.

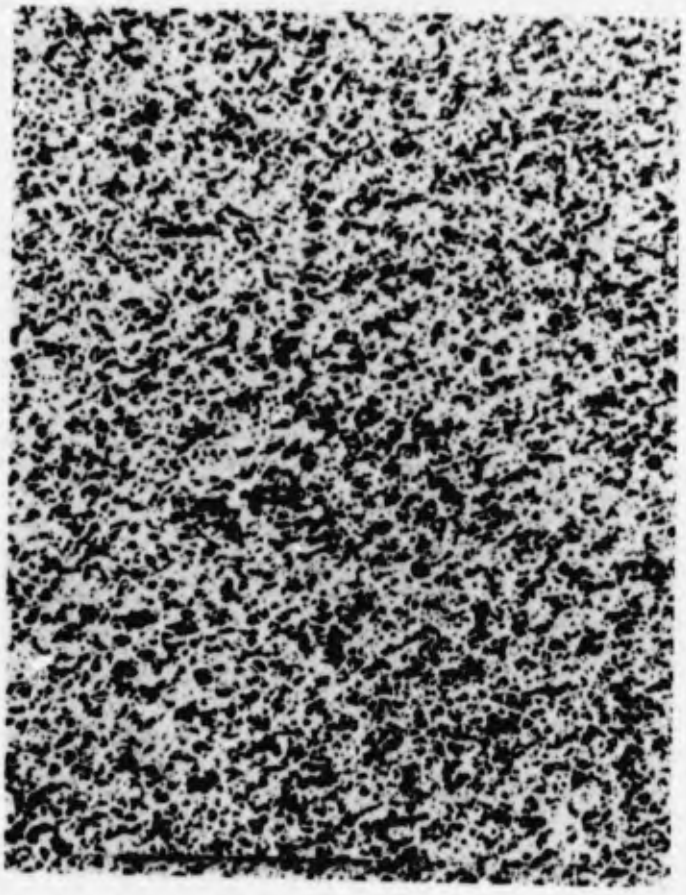

Fig. 6 - SiC R-69. As polished, 200X. Incomplete densification caused by low boron content.

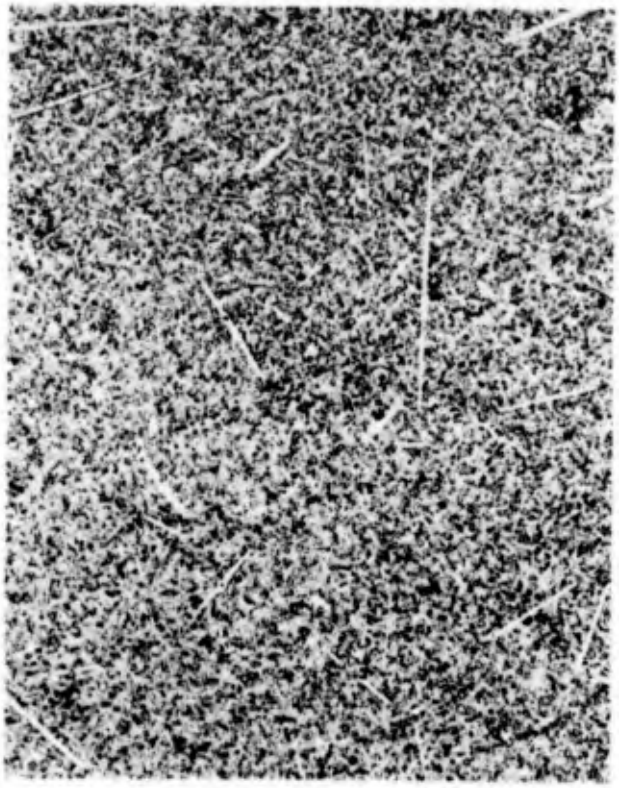

Fig. 7 - SiC R-59. 200X, thermal etch. Exaggerated grain growth in powder ES-3.

Fig. 8 - SiC R-59, 1000X, Thermal etch.
Exaggerated grain growth in Powder ES-3.

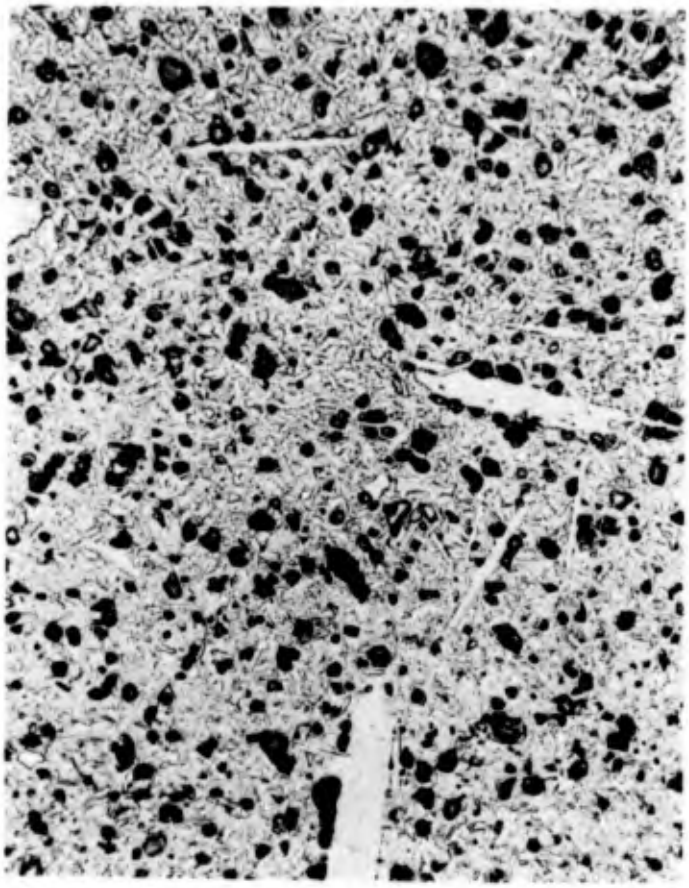

Fig. 9 - SiC R-60 at 1900°C. 500X, thermal etch. Exaggerated grain growth below the sintering temperature in powder ES-3.

Fig. 10 - SiC R-71, as polished, 500X. High residual porosity caused by exaggerated grain growth.

Fig. 11 - SiC R-59 as polished, 1500X. Silicon phase in the vicinity of large tabular grains of SiC.

Fig. 12 - SiC R-74, 100X, thermal etc. Impinging and interpenetrating tabular crystals. Trapped pores.

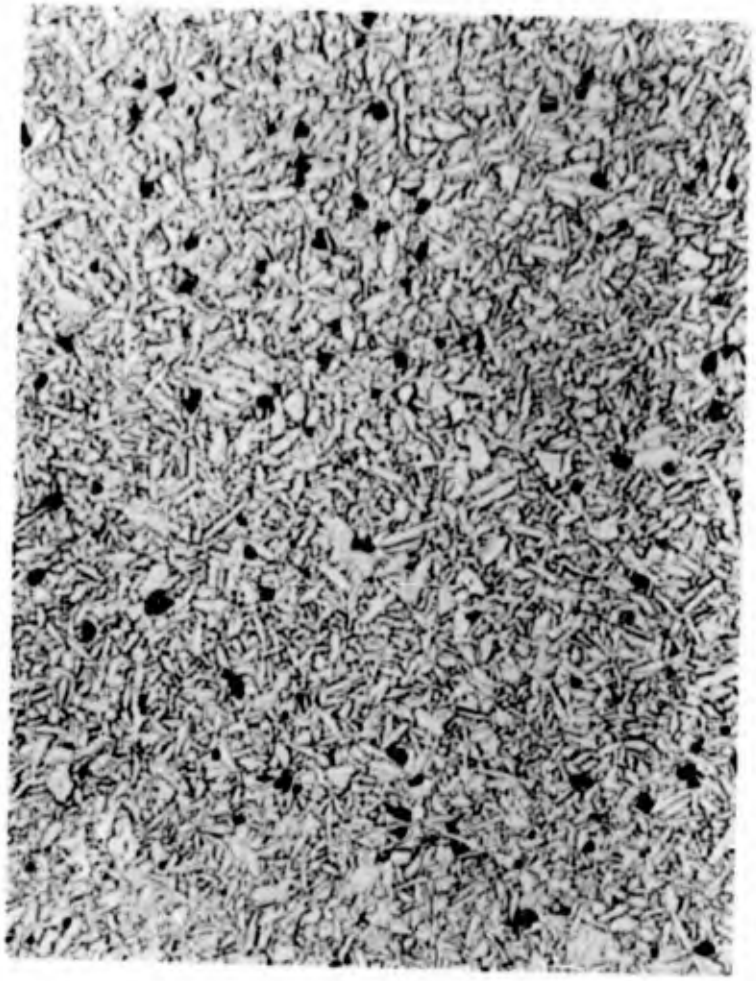

Fig. 13 - SiC R-75, 1000X, thermal etch. Exaggerated grain growth suppressed by carbon addition. Carbon grains. Compare Fig. 12.

Fig. 14 - SiC R-30, 10,000X, chemical etch, double-stage replica. Microstructure composed of equiaxed grains, typical for oxygen-rich powders.

Fig. 15 - SiC R-42, 30,000X, thermal etch, double-stage replica. Equiaxed uniform grains typical for oxygen-rich powders. Note traces of twin boundaries.

Fig. 16 - SiC R-42, 30,000X, HF etch, double-stage replica. Selectively revealed SiO_2 phase.

Fig. 17 - SiC R-30, X65,000. TEM. Silica phase in SiC.

Fig. 18 - SiC R-48, X1000, thermal etch. Moderate case of exaggerated grain growth.

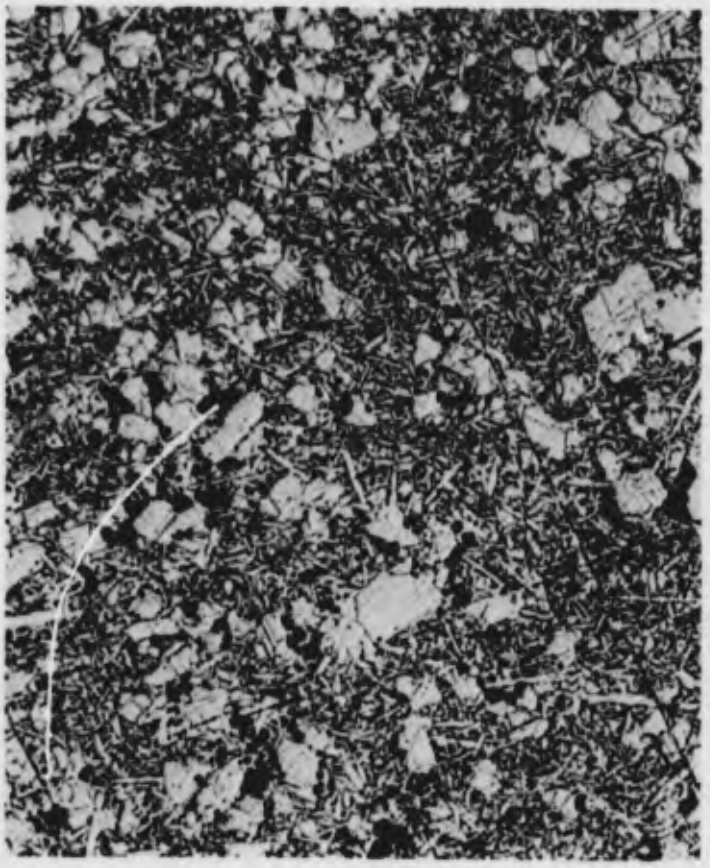

Fig. 19 - SiC R-83, X500, thermal etch. Morphology of large β-SiC grains grown on hot-pressing, after carbon addition.

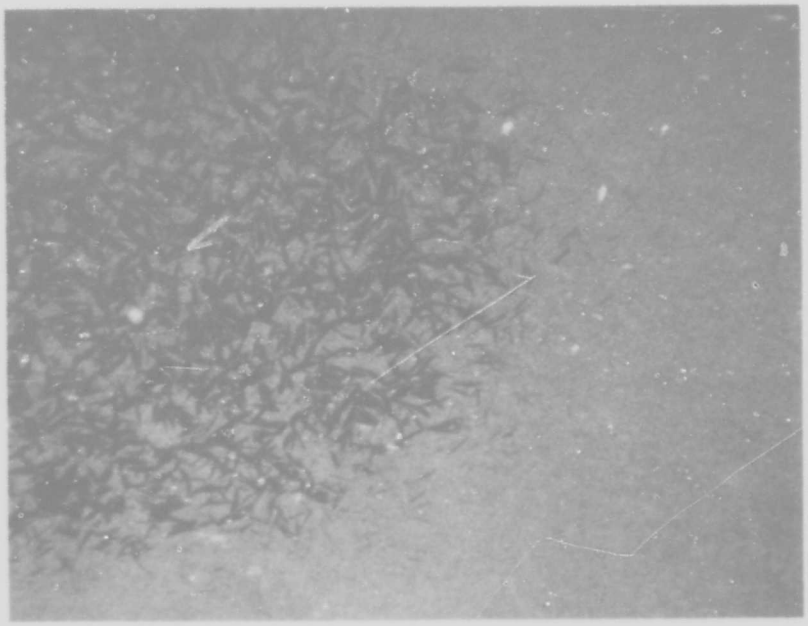

Fig. 20 - SiC R-84, thermal etch, 25X. Exaggerated grain growth localized in the core of a pressing.

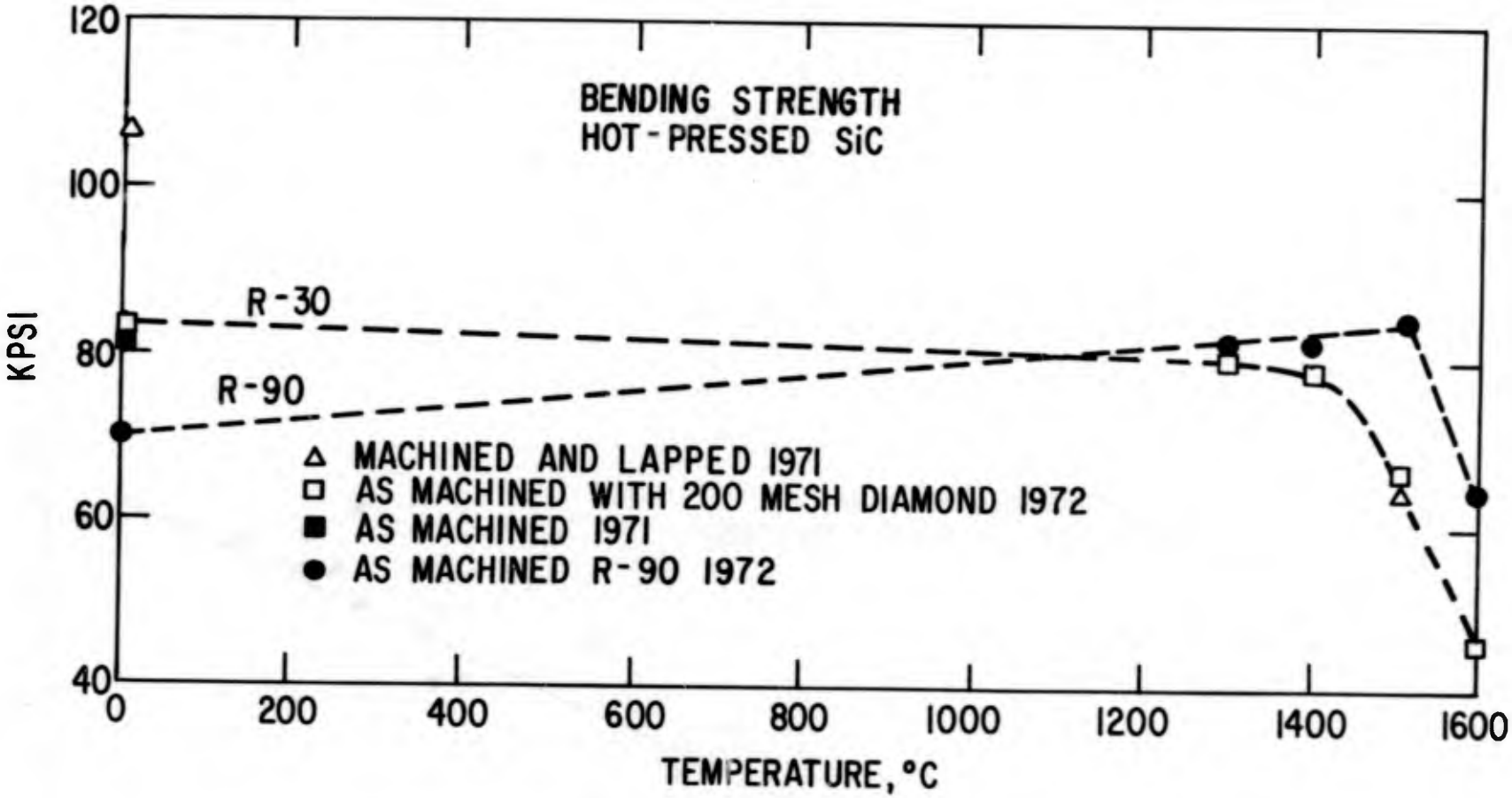

Fig. 21 - Strength-temperature relationship for two fine-grained SiC materials.

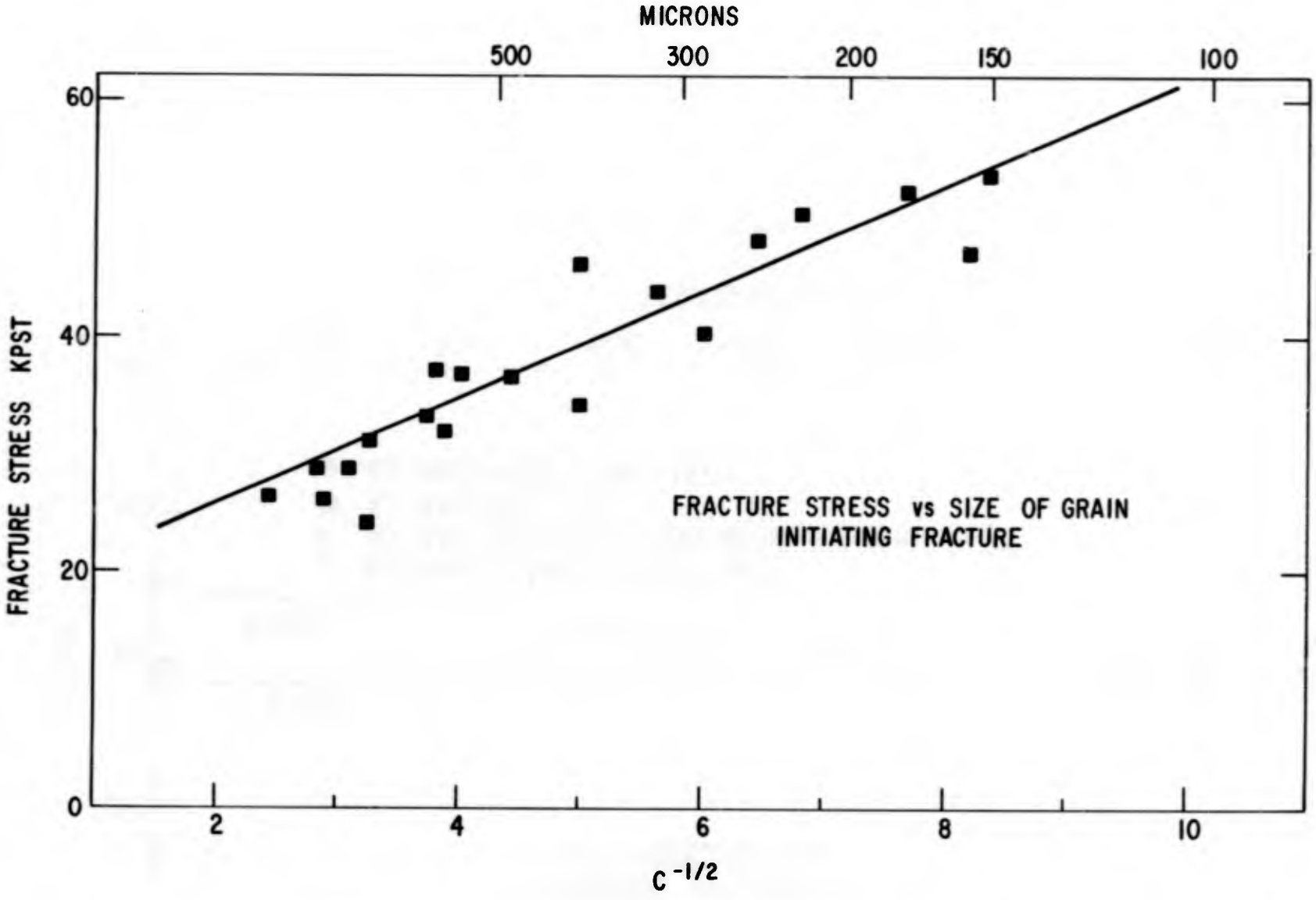

Fig. 22 - Fracture stress of SiC R-63 vs. size of grain initiating fracture.

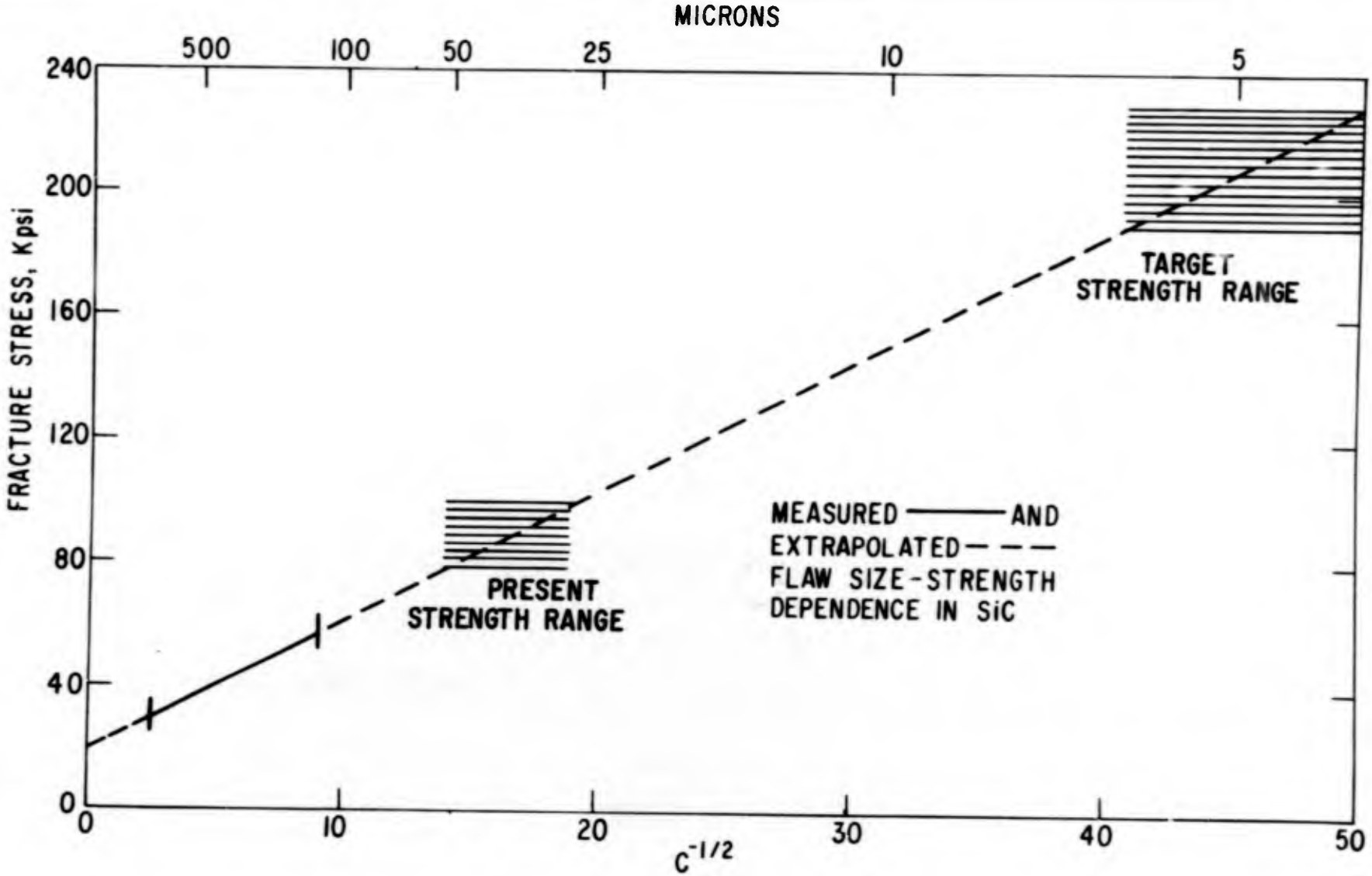

Fig. 23 - Extrapolated flaw size-strength dependence in SiC.

CREEP TEST ASSEMBLY SCHEMATIC

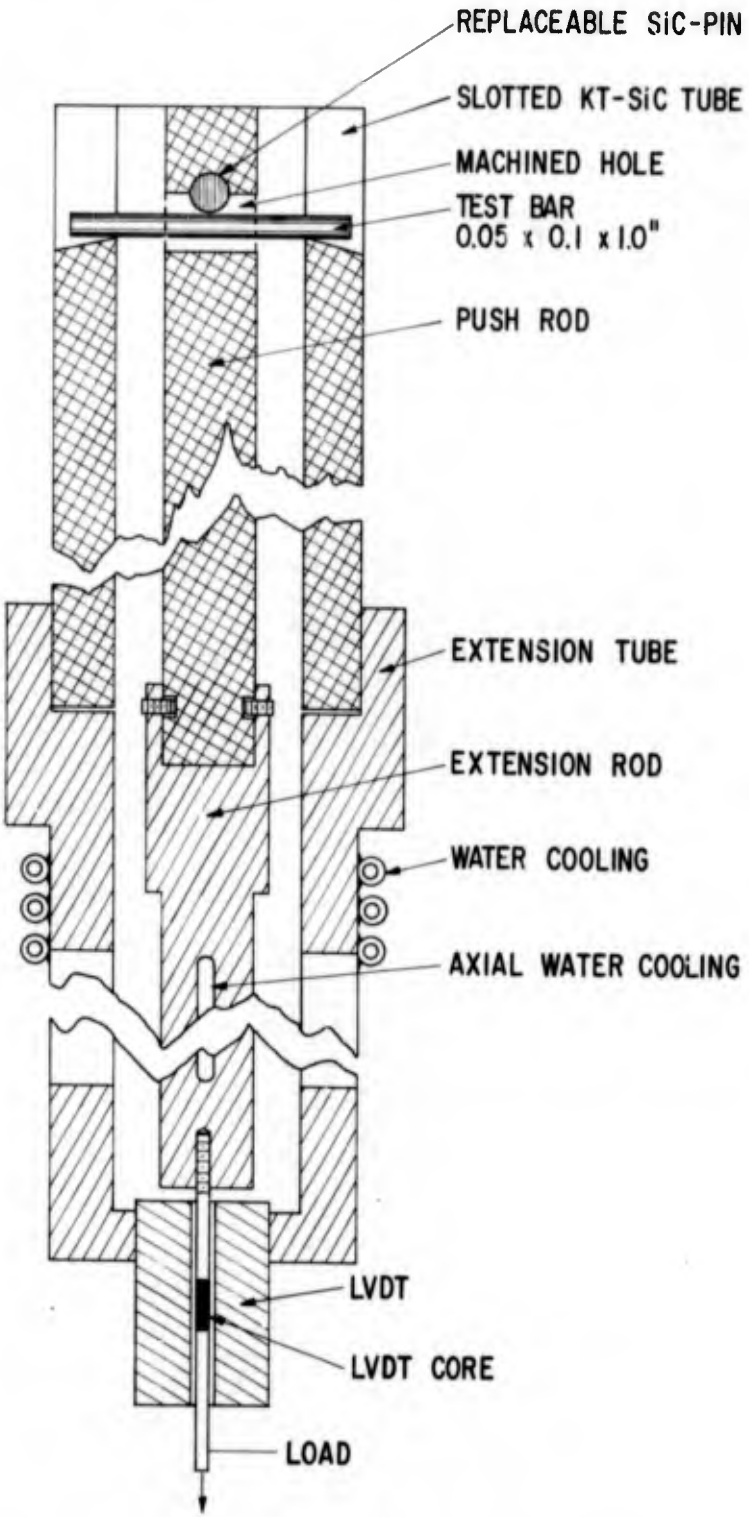

Fig. 24 - SiC Grips for creep measurement.

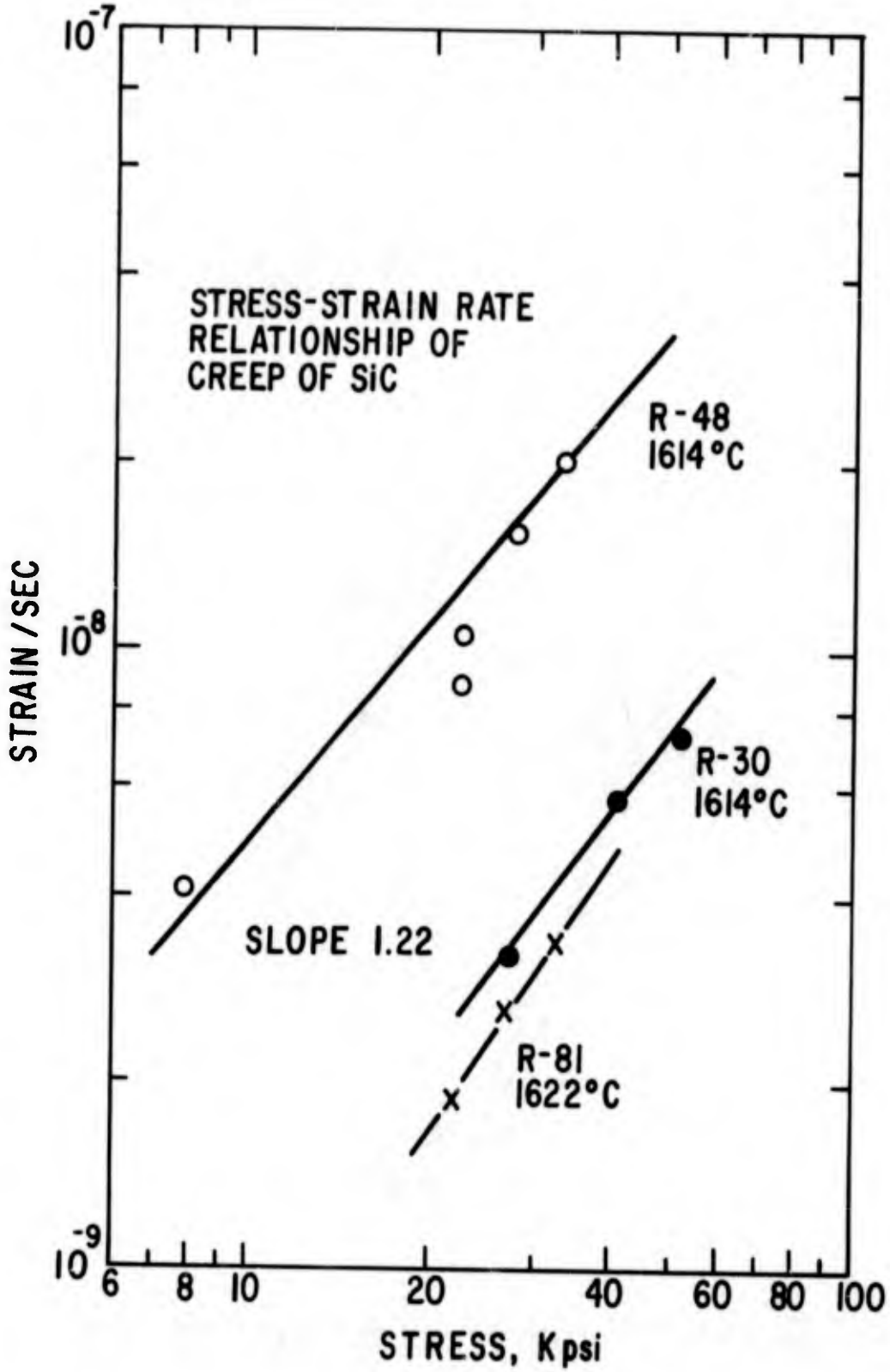

Fig. 25 - Strain rate - Stress relationship in three SiC specimens.

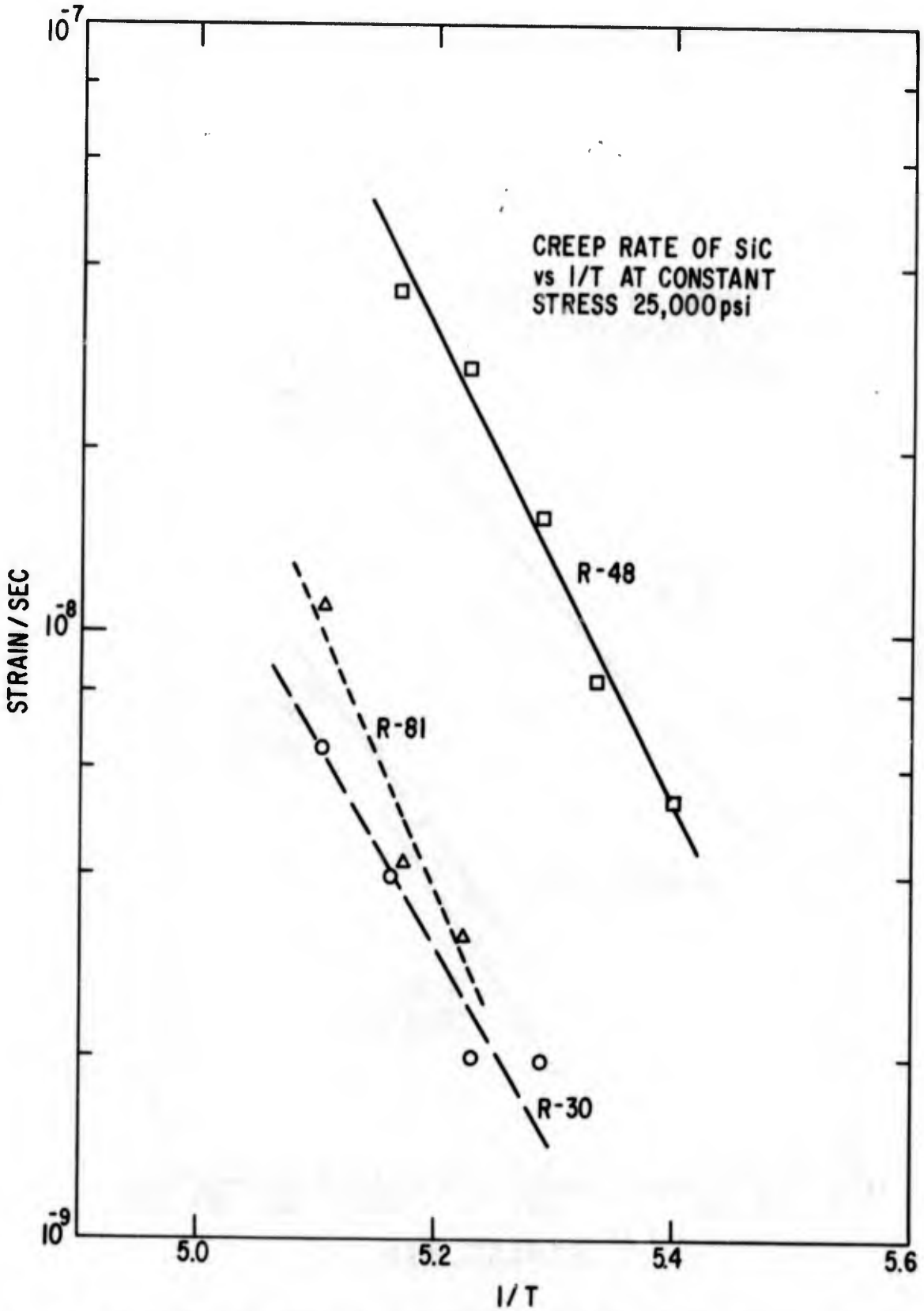

Fig. 26 - Creep of three SiC specimens vs. 1/T at constant stress 25,000 psi.

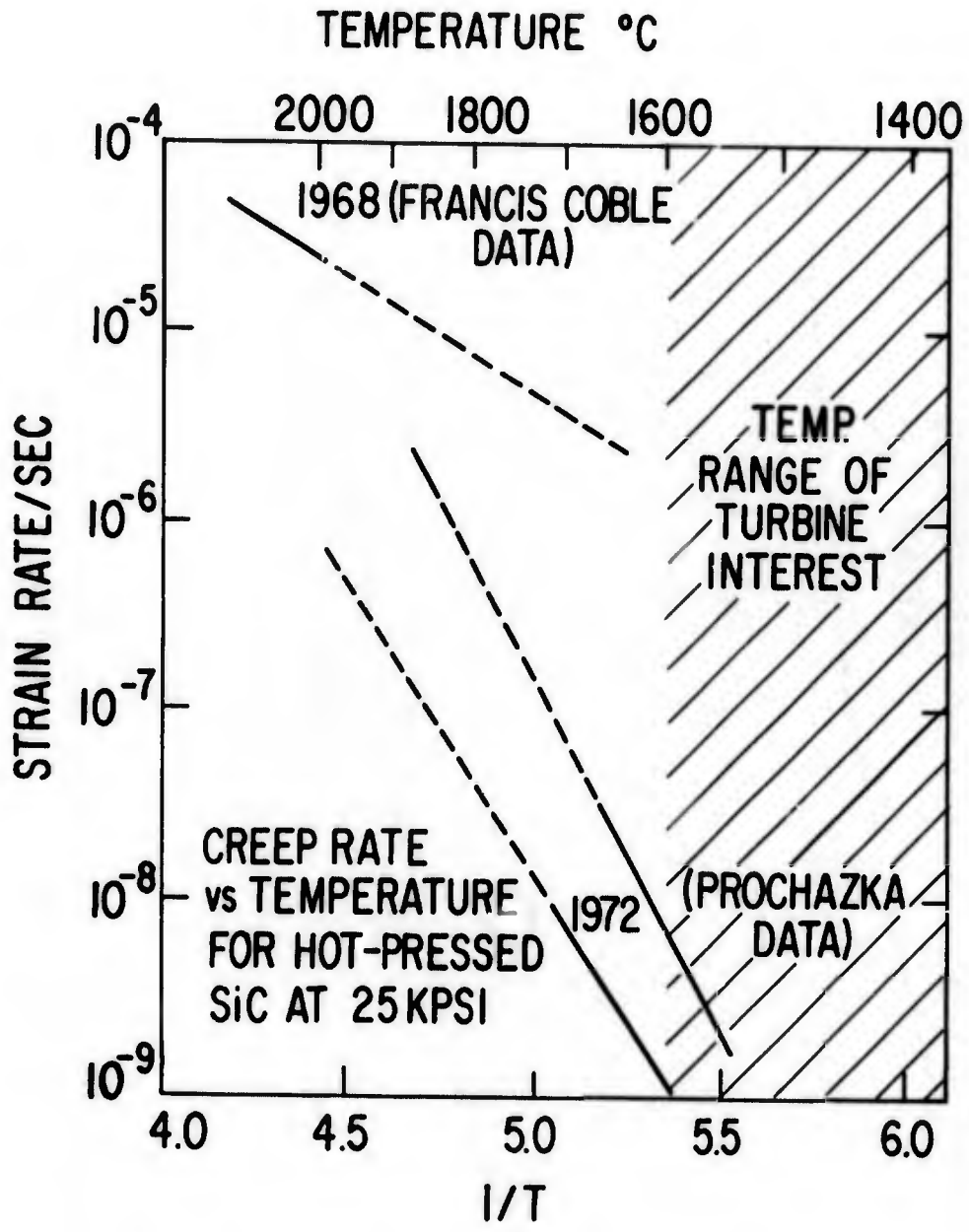

Fig. 27 - Measured and extrapolated creep rate data.

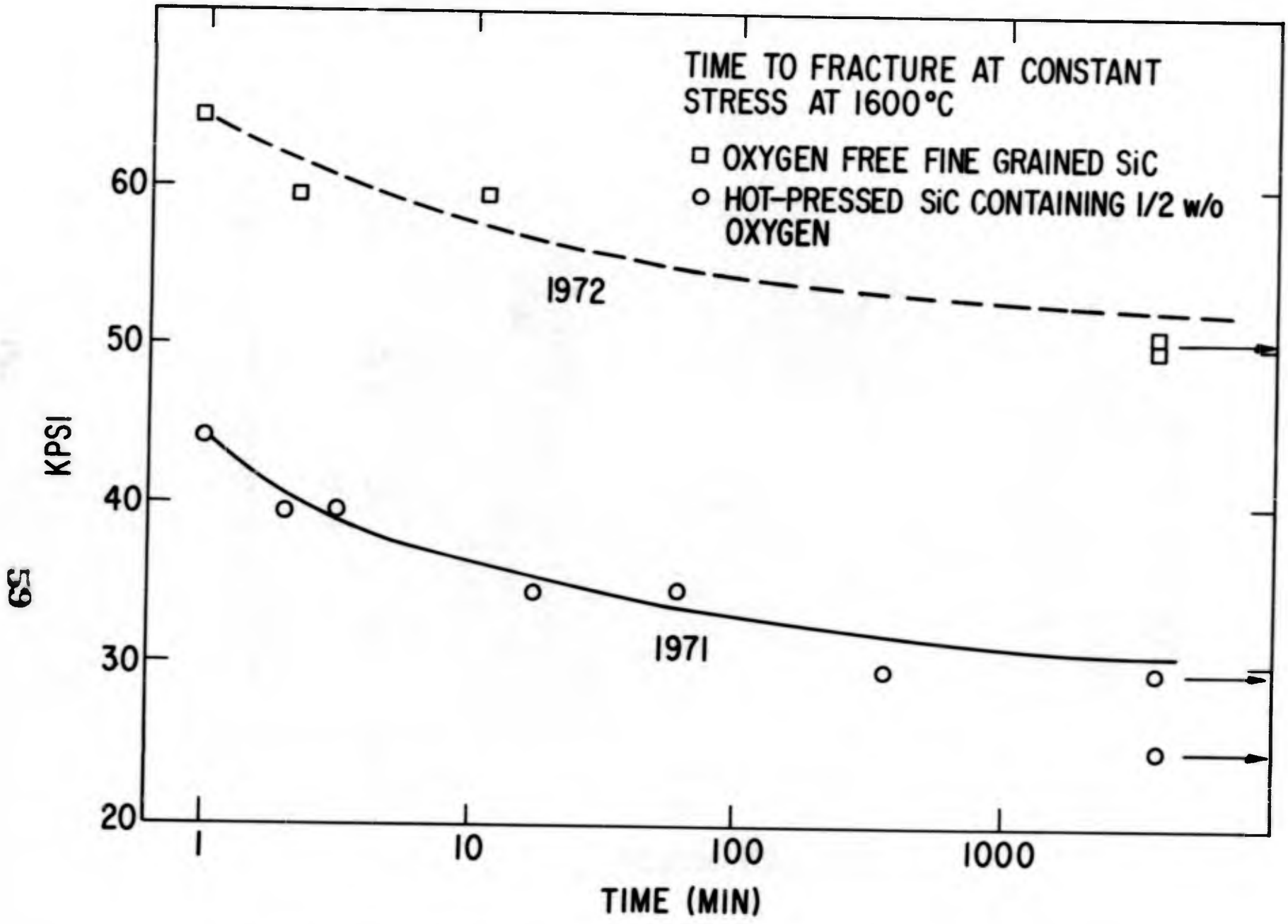

Fig. 28 - Fracture stress vs. time-to-fracture for two fine-grained SiC specimens.

Fig. 29 - Slowly propagating crack at σ_f = 30,000 psi and 1600°C revealed on the fracture surface of hot-pressed SiC R-30.

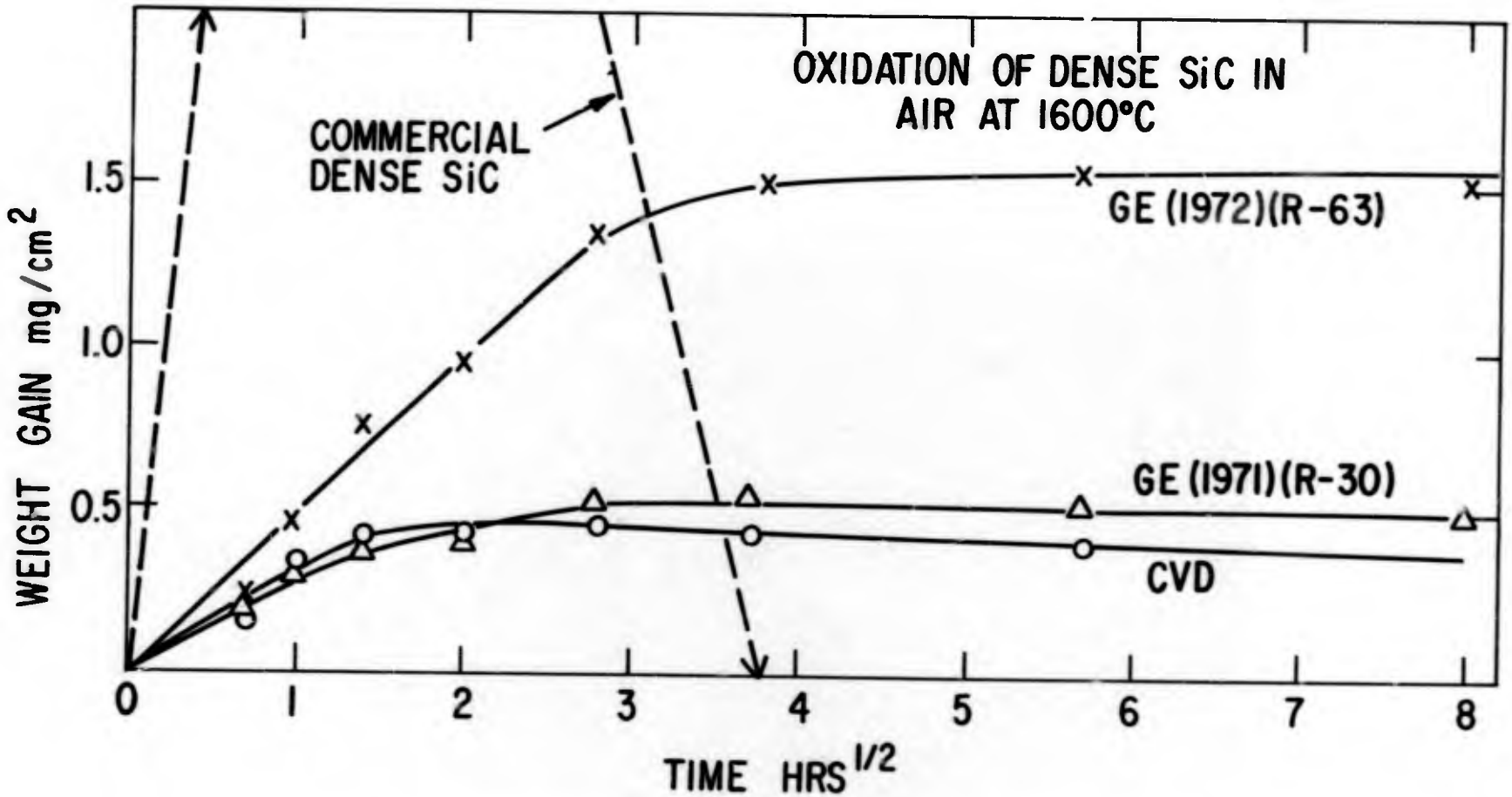

Fig. 30 - Oxidation of dense silicon carbide at 1600°C in air.

OXIDATION BEHAVIOR OF DENSE SiC

64 HOURS EXPOSURE IN AIR AT 1600°C

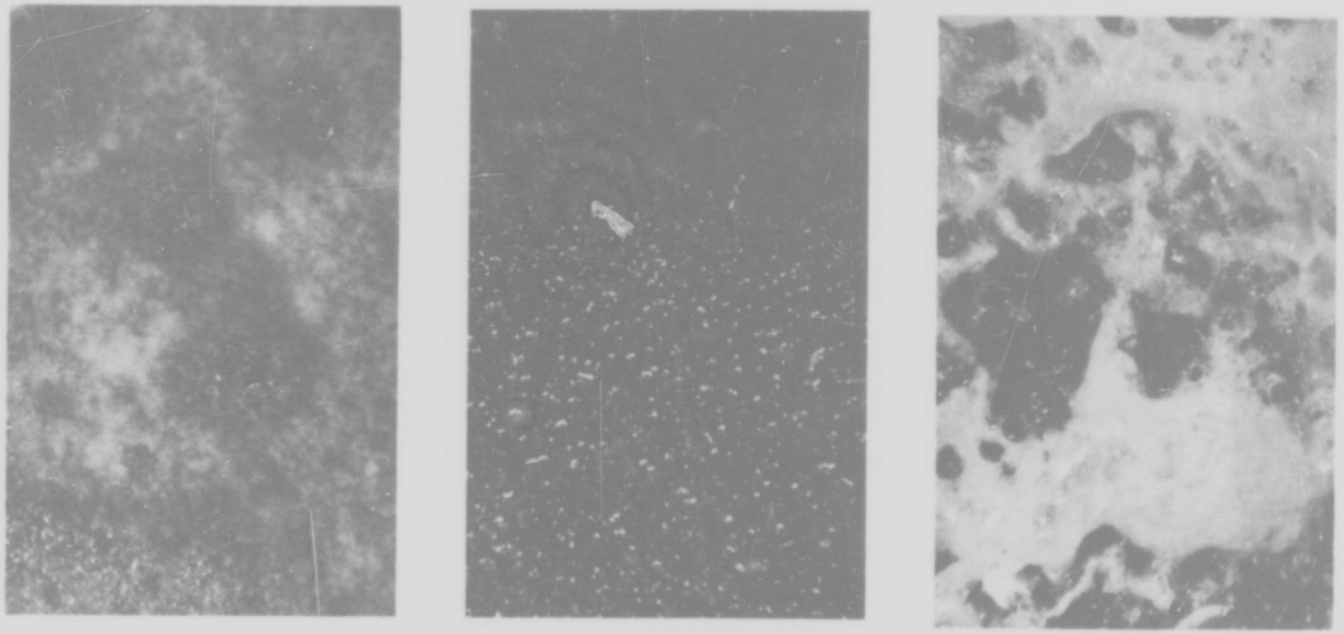

CR&D R-63
+ 1.5 MG/CM²

CR&D R-30
+ 0.53 MG/CM²

COMMERCIAL SiC
HEAVILY ATTACKED

Fig. 31 - Surface of three hot-pressed SiC exposed 64 hours to 1600°C in air. 50X.